AD-765 723

DYNAMIC TENSILE FAILURE IN ROCKS

STANFORD RESEARCH INSTITUTE

PREPARED FOR

DEFENSE ADVANCED RESEARCH PROJECTS AGENCY

BUREAU OF MINES, TWIN CITIES, MINNESOTA

TWIN CITIES MINING RESEARCH CENTER

JUNE 1973

DISTRIBUTED BY:

NTIS

National Technical Information Service

U. S. DEPARTMENT OF COMMERCE

Final Report *June 1973*

DYNAMIC TENSILE FAILURE IN ROCKS

By: DONALD A. SHOCKEY, CARL F. PETERSEN, DONALD R. CURRAN, JOHN T. ROSENBERG, and LYNN SEAMAN

Prepared for:

BUREAU OF MINES
TWIN CITIES MINING RESEARCH CENTER
TWIN CITIES, MINNESOTA 55111
Attention: DR. D. E. SISKIND

CONTRACT H0220053

Sponsored by

ADVANCED RESEARCH PROJECTS AGENCY

STANFORD RESEARCH INSTITUTE
Menlo Park, California 94025 · U.S.A.

Final Report *June 1973*

DYNAMIC TENSILE FAILURE IN ROCKS

By: DONALD A. SHOCKEY, CARL F. PETERSEN, DONALD R. CURRAN, JOHN T. ROSENBERG, and LYNN SEAMAN

Prepared for:

BUREAU OF MINES
TWIN CITIES MINING RESEARCH CENTER
TWIN CITIES, MINNESOTA 55111
Attention: DR. D. E. SISKIND

CONTRACT H0220053

Sponsored by

ADVANCED RESEARCH PROJECTS AGENCY

STANFORD RESEARCH INSTITUTE
Menlo Park, California 94025 · U.S.A.

UNCLASSIFIED
Security Classification

DOCUMENT CONTROL DATA - R & D

(Security classification of title, body of abstract and indexing annotation must be entered when the overall report is classified)

1. ORIGINATING ACTIVITY (Corporate author): STANFORD RESEARCH INSTITUTE

2a. REPORT SECURITY CLASSIFICATION: UNCLASSIFIED

2b. GROUP:

3. REPORT TITLE: DYNAMIC TENSILE FAILURE IN ROCKS

4. DESCRIPTIVE NOTES (Type of report and inclusive dates): Final Report - February 14, 1972 to August 26, 1973

5. AUTHOR(S) (First name, middle initial, last name): Donald A. Shockey, Carl F. Petersen, Donald R. Curran, John T. Rosenberg, and Lynn Seaman

6. REPORT DATE	7a. TOTAL NO. OF PAGES	7b. NO. OF REFS
June 26, 1973	72	22

8a. CONTRACT OR GRANT NO.: H0220053

b. PROJECT NO.: ARPA Code Number 1579, Amendment 3

c. Program Code Number 2F10

d.

9a. ORIGINATOR'S REPORT NUMBER(S): PYU-1793

9b. OTHER REPORT NO(S) (Any other numbers that may be assigned this report):

10. DISTRIBUTION STATEMENT: Distribution of this Document is Unlimited.

11. SUPPLEMENTARY NOTES:

12. SPONSORING MILITARY ACTIVITY: Defense Advanced Research Projects Agency, Washington, D.C.

13. ABSTRACT (Summary)

The results of a two-year program on dynamic fracture behavior of rocks are described. The goal was to develop the capability to predict the fragment size distribution of rock resulting from known dynamic loads. This goal has been largely realized for a simple, well-characterized rock type, Arkansas novaculite, under one-dimensional-strain impact loading. A gas gun was used to accelerate flat plates against flat rock specimens. Ytterbium piezoresistive stress gages were used to measure stress histories, and the dynamic tensile strength and fragment size distributions were determined. The mechanism of fragmentation was deduced from fractographic observations on impacted specimens.

A computational fragmentation model was developed that treats quantitatively the four stages of the hypothesized fragmentation mechanism: (1) activation of inherent flaws, (2) crack growth, (3) crack coalescence, and (4) fragmentation. This model was inserted into a one-dimensional, finite difference wave propagation computer code to obtain a capability to predict the fragment size distribution.

The required input parameters include the load history and such rock specific properties as the initial flaw size distribution, the fracture toughness, and the crack growth velocity. These material parameters were determined for Arkansas novaculite, and a calculation was made to simulate the conditions of a dynamic impact experiment. The calculated and experimental fragment size distributions (Figure 12) are in qualitative agreement, and indicate that it is feasible to make successful

UNCLASSIFIED

Security Classification

KEY WORDS	LINK A ROLE	LINK A WT	LINK B ROLE	LINK B WT	LINK C ROLE	LINK C WT
Dynamic tensile test						
Tensile strength						
Novaculite						
Fracture toughness						
Gas gun						
Fragmentation						
Fragmentation size distribution						
Computational model						

Abstract (Summary) concluded

predictions of rock fragmentation based on knowledge of a few measurable rock properties. Characterization work on Sioux quartzite, Holston limestone, and Westerly granite was begun.

DD FORM 1 NOV 65 1473 (BACK)
(PAGE 2)

UNCLASSIFIED

Security Classification

STANFORD RESEARCH INSTITUTE
Menlo Park, California 94025 · U.S.A

Final Report *June 1973*

DYNAMIC TENSILE FAILURE IN ROCKS

By: DONALD A. SHOCKEY, CARL F. PETERSEN, DONALD R. CURRAN, JOHN T. ROSENBERG, and LYNN SEAMAN

Prepared for:

BUREAU OF MINES
TWIN CITIES MINING RESEARCH CENTER
TWIN CITIES, MINNESOTA 55111

Attention: DR. D. E. SISKIND

SRI Project PYU-1793

ARPA Code Number:	1579, Amendment 3	Contract Number:	H0220053
Program Code Number:	2F10	Principal Investigator:	Dr. Carl F. Petersen
Name of Contractor:	Stanford Research Institute	Phone Number:	(415) 326-6200, Ext. 4814
Date of Contract:	April 6, 1972	Project Scientist:	Dr. Donald A. Shockey
Contract Expiration Date:	June 26, 1973	Phone Number:	(415) 326-6200, Ext. 2587
Amount of Contract:	$59,598	Short Title of Work:	Dynamic Tensile Failure in Rocks

Approved by:

G. R. ABRAHAMSON, *Director*
Poulter Laboratory

C. J. COOK, *Executive Director*
Physical Sciences Division

Sponsored by

ADVANCED RESEARCH PROJECTS AGENCY

ACKNOWLEDGMENTS

This work was sponsored under Contracts H0210018 and H0220053 and was monitored by D.E. Siskind of the U. S. Bureau of Mines, Twin Cities Research Center.

The success of this program is due to a true team effort. Many of our colleagues contributed significantly to the work reported here.

David Erlich supervised the dynamic impact experiments on Westerly granite.

Paul De Carli tried various techniques for revealing the inherent flaw structure in Sioux quartzite, Westerly granite, and pink Tennessee marble.

Dante Petro sectioned the impacted rock specimens skillfully and provided excellent micrographs.

B. Samuel Holmes made valuable suggestions for the development of the fragmentation theory.

R. Sedlacek measured the quasi-static tensile strength of Arkansas novaculite and Sioux quartzite.

CONTENTS

Preceding page blank

LIST OF ILLUSTRATIONS

LIST OF TABLES

SUMMARY

The results of a two-year program on dynamic fracture behavior of rocks are described. The goal was to develop the capability to predict the fragment size distribution of rock resulting from known dynamic loads. This goal has been largely realized for a simple, well-characterized rock type, Arkansas novaculite, under one-dimensional-strain impact loading. A gas gun was used to accelerate flat plates against flat rock specimens. Ytterbium piezoresistive stress gages were used to measure stress histories, and the dynamic tensile strength and fragment size distributions were determined. The mechanism of fragmentation was deduced from fractographic observations on impacted specimens.

A computational fragmentation model was developed that treats quantitatively the four stages of the hypothesized fragmentation mechanism: (1) activation of inherent flaws, (2) crack growth, (3) crack coalescence, and (4) fragmentation. This model was inserted into a one-dimensional, finite difference wave propagation computer code to obtain a capability to predict the fragment size distribution.

The required input parameters include the load history and such rock specific properties as the initial flaw size distribution, the fracture toughness, and the crack growth velocity. These material parameters were determined for Arkansas novaculite, and a calculation was made to simulate the conditions of a dynamic impact experiment. The calculated and experimental fragment size distributions (Figure 12) are in qualitative agreement, and indicate that it is feasible to make successful quantitative predictions of rock fragmentation based on knowledge of a few measurable rock properties. Characterization work on Sioux quartzite, Holston limestone, and Westerly granite was begun.

I INTRODUCTION

Rock fragmentation under high rate load applications is a little-understood phenomenon. There is at present no satisfactory theoretical basis for predicting dynamic fracture behavior, although such a capability would be very useful in the solution of many practical mining and civil engineering problems. For example, rapid excavation could be done more safely and economically, the stability of structures in rock could be designed and evaluated with more confidence, and the efficiency of rock disintegration processes could be improved. It was with this motivation that the work described in this report was undertaken.

Our goal was to develop a capability for predicting the fragment size distribution in rock resulting from dynamic loads. We limited the main effort to a simple, well characterized, homogeneous rock type, Arkansas novaculite, under one-dimensional-strain loading. The approach consisted of the following steps:

- Impact experiments were performed on a homogeneous rock under well-controlled conditions, and the fracture behavior under various dynamic load histories was studied.
- Observations were made on impacted specimens to establish the physical processes underlying rock fragmentation.
- A computational model of the fragmentation process was constructed based on experimental evidence to predict the fragment size distribution resulting from a given load history.
- Rock properties needed for the model were measured.
- The model was inserted into a wave propagation code and calculations were performed. The results were compared with experimental results.

This report is organized into six chapters. Chapter II describes the impact experiments, the experimental and calculational methods used to determine the stress history in the specimens, and the extent of fracture and fragmentation of the specimens. Chapter III presents petrographic and fractographic observations made on the impacted specimens; this evidence is used to deduce the mechanism of fragmentation, i.e., the sequence of microprocesses which occur in the specimens during loading and result in fragmentation. In Chapter IV a computational model of rock fragmentation under those loading conditions is constructed to describe the resulting fragment size distribution. The model is based on the hypothesized fragmentation mechanism and requires the loading history and certain rock properties as input. In Chapter V, the rock properties that control the fragmentation behavior (the initial flaw size distribution, the fracture toughness, and the velocity of crack growth) are determined in Arkansas novaculite. In Chapter VI the results of the calculations are presented and compared with the measured results. The results of characterization work on three other rock types are presented in the ppendix.

The essential results of this work may be quickly grasped by comparing figures showing experimentally observed crack patterns and measured fragment size distributions for novaculite (Figures 4 and 6, respectively) with the corresponding calculational results shown respectively in Figures 11 and 12. The agreement is considered good, and indicates that the approach taken here could lead to a useful solution to the problems of rock fragmentation under dynamic loads.

II IMPACT EXPERIMENTS

Material

Arkansas novaculite, a naturally occurring polycrystalline quartzite, was chosen as the baseline material for this study because of its simplicity. It is pure, dense, and homogeneous, and consists of equisized, equiaxed and randomly oriented quartz grains having an average diameter of about 10 μm. A population of flat flaws exists on planes roughly parallel to each other. The structural and mechanical properties of novaculite are presented and discussed more fully in Chapter V.

Impact Loading Procedure

Controlled impact experiments on novaculite were carried out with a gas gun using a flat projectile impact technique, so that fracture and fragmentation occurred under one-dimensional strain conditions.

Projectiles, 30.5 cm long by 6.35 cm in diameter for the smaller gas gun and 76.2 cm long by 10.2 cm in diameter for the larger, were accelerated down the evacuated barrel of the gun by the sudden release of pressure from an adjacent pressurized chamber of helium. Flat target specimens were impacted with thin polyethylene or plexiglass flyer plates attached to the front end of the projectiles (Figure 1). Under such flat plate impact, compressive waves initially run into the specimen and projectile head to produce a state of one-dimensional compressive strain. Tension is produced in the specimens when release waves running inward from the free surface of the specimen meet similar release waves running inward from the back surface of the flyer plate. From a knowledge of the shock impedance (product of density and shock velocity) of the rock and flyer plate, the stresses in the rock specimen can be calculated. A sufficiently large diameter-to-thickness ratio for the specimen ensures that the tensile strain is one-dimensional by preventing unloading waves from the specimen periphery from reaching the interior during the tension phase.

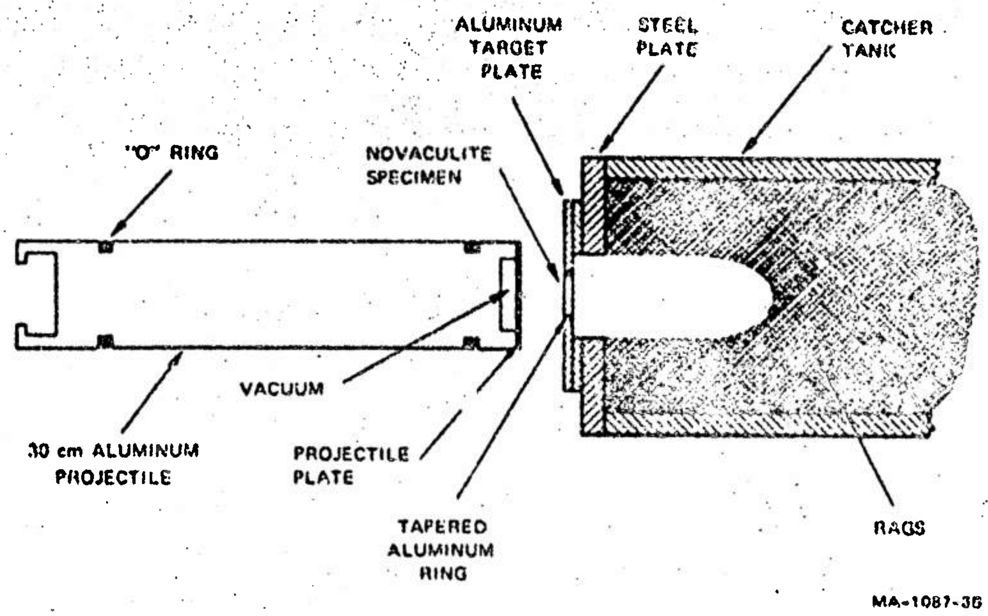

FIGURE 1 EXPERIMENTAL ARRANGEMENT FOR HIGH RATE TENSILE TESTING OF CYLINDRICAL ROCK SPECIMENS IN A GAS GUN

The target specimens were short cylinders, usually about 0.635 cm thick and 1.27 to 3.81 cm in diameter. Their axes were carefully aligned to coincide with that of the gun barrel to ensure flat plate impact. The specimens were fit tightly into constraining rings of aluminum, which is a very close match to novaculite in shock impedance. Most of the aluminum constraining rings had an 8-degree taper on the outer circumference and were press-fitted into a larger aluminum plate serving as a specimen holder. Others had no taper and were lightly held in the specimen holder by several dabs of epoxy. Upon impact with the flyer plate, the specimen and constraining ring fly free from the aluminum holder and into a catcher tank, which is filled with rags to prevent subsequent impacts and possible uncontrolled damage. The projectile and projectile head are prevented from entering the catcher tank by the steel plate.

Fifty-three tensile experiments on Arkansas novaculite at high loading rates were performed using the gas guns. Fourteen of these were instrumented with ytterbium stress gages to determine stress histories and to measure the magnitudes of recompression waves produced by fracture.[1] An additional twenty were uninstrumented experiments in which we attempted to determine the dynamic fracture strength of novaculite and any effects of orientation on fracture strength,[1,2] whereas ten others were performed on jacketed specimens to study fragmentation behavior. The remaining nine experiments were either of a preliminary nature, to determine in a rough way the impact velocities and other experimental conditions required to carry out the proposed program, or of an investigative nature to determine, for example, the reason for the occurrence of undesirable radial cracking.

Determination of Dynamic Tensile Strength

A series of 20 uninstrumented experiments was performed to measure the dynamic tensile strength of novaculite, to determine the effect of specimen orientation on the dynamic fracture strength, and to produce fracture surfaces for examination in the scanning electron microscope to gain information concerning the fracture mechanism.

Ten specimens were cut so that the impact direction was normal to the planes of the inherent flaws; specimens in the remaining 10 were oriented so that the impact direction was parallel to the flaw planes. All specimens were 1.27 cm in diameter by 0.635 cm thick and press-fitted into 3.81 cm diameter by 0.635 cm aluminum annuli. The outher periphery of each annulus was provided with an 8-degree taper to facilitate ejection upon impact of the specimen-ring assembly from the aluminum target plate.

Very extensive cracking, usually resulting in comminution and loss of one or both sides of the specimen from the aluminum annulus, was produced in all of the first nine experiments even at stresses as low as 20 MN/m^2 (2900/psi).* This initially puzzling behavior was prevented in the subsequent 11 shots by lightly tacking the tapered annuli to the target plates in three or four places with epoxy instead of press-fitting. In the latter experiments no radial cracking occurred, and a good estimate of the dynamic fracture strength was obtained.

The results of this series of experiments are presented in Table 1. The dynamic tensile strength was taken as the average of the highest stress at which no damage could be observed on diametrical sections of the specimen, and the lowest stress at which incipient spallation occurred. A cross-sectional view of incipient spallation is provided in Figure 2. For the parallel specimen orientation, Specimen 36 did not crack at 39.4 MN/m^2 (5710 psi) but Specimen 35 did crack at 43.5 MN/m^2 (6300 psi); for the normal specimen orientation, no cracking was observed in Specimen 43, which was subjected to a peak tensile stress of 38.8 MN/m^2 (5630 psi), whereas Specimen 37 showed cracking at 42.6 MN/m^2 (6180 psi). Thus the dynamic tensile strength of novaculite in the direction normal to the planes of inherent cracks is 40.6 ± 2.0 MN/m^2 (5890 ± 290 psi); the dynamic strength in the parallel direction is 41.4 ± 2.0 MN/m^2 (6000 ± 290 psi).

---

*Standard International (S.I.) units, as now required by many government agencies and professional societies for technical reports, papers and journals will be used in this report. For convenience, however, English units will also be given in parentheses directly thereafter. Stress equivalents to slide rule accuracy are as follows: 1 Megapascal (MN/m^2) = 10^6 N/m^2 = 10.2 kg/cm^2 = 145 psi = 10 bar.

Table 1

DYNAMIC TENSILE STRENGTH EXPERIMENTS

Experiment No.	Specimen Orientation	Impact Velocity (m/sec)	Maximum Peak Tensile Stress* (MN/m^2)	Extent of Damage
33	P	12.2	33.3	No damage.
34	N	12.0	32.8	No damage.
35	P	15.9	43.4	1 spall crack about half specimen diameter.
36	P	14.4	39.4	No damage.
37	N	15.6	42.6	4 spall cracks on sectioned surface.
38	N	18.5	50.5	2 spall cracks on sectioned surface.
39	N	23.4	64.0	3 spall cracks on sectioned surface.
40	N	18.0	49.2	1 spall crack on sectioned surface.
41	N	16.8	46.0	No damage.
42	N	17.0	46.4	1 spall crack.
43	N	14.2	38.8	No damage.

Notes: The tapered Al annuli were held lightly in place with four dabs of epoxy.

Three experiments provided meaningful dynamic fracture strength values.

P = specimen orientation was such that flaws preexisting in the rock lay roughly parallel to the impact direction.

N = specimen orientation was such that flaws preexisting in the rock lay normal to the impact direction.

* Calculated from the measured impact velocity as described in Reference 1

$\frac{\Delta\sigma}{\sigma} \simeq 4\%$.

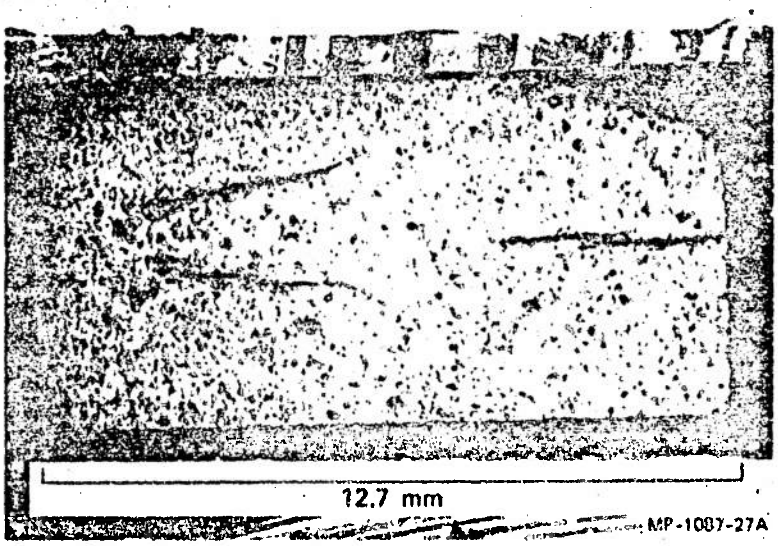

FIGURE 2 CROSS-SECTIONAL VIEW OF SPECIMEN 30 SHOWING INCIPIENT SPALLATION

We conclude that the dynamic tensile strength of Arkansas novaculite is insensitive to the orientation of preexisting flaws. In view of the pronounced flaw orientation anisotropy of novaculite, the fracture strength isotropy is surprising.

Determination of Fragment Size Distribution

At low impact velocities (less than about 20 m/sec), Arkansas novaculite specimens could sustain considerable fracture damage while maintaining integrity. At impact velocities sufficient to cause fragmentation, a method was required to prevent the fragments from scattering and thereby resulting in possible damage and loss of the fragments. The arrangement used for recovering heavily damaged specimens entailed encasing the cylindrical rock specimens completely in a much tougher material of similar shock impedance. Aluminum was found to be a suitable encasing material, first, because it does not undergo brittle fracture under the loading conditions of these experiments and therefore contains the cracking and fragmenting rock specimen, and, second, because its shock impedance is very similar to that of novaculite, so that disturbance of stress waves as they cross the specimen-encasement interface is minimal. The dimensions of the targets were designed to reduce edge effects.

As shown in Figure 3, specimens of Arkansas novaculite 1.27 cm in diameter by 0.635 cm thick were fit tightly in the center of an aluminum disk 5.08 cm in diameter and 0.953 cm thick. An aluminum cover plate 5.08 cm in diameter by 0.318 cm thick was then placed over the exposed end of the specimen and held firmly to the disk with four equally spaced screws. An epoxy was applied to the specimen surface adjacent to the cover plate to ensure intimate contact with the aluminum casing. This target assembly was then subjected to flat-plate impact with the gas gun.

Ten experiments were carried out; the details are given in Table 2. It was planned to subject Specimens 44, 45, and 46 to stresses a factor of about 2.0, 1.5, and 1.25 in excess of the dynamic tensile strengths in an attempt to obtain various degrees of crack coalescence leading to fragmentation. The resulting fracture damage is described in the next section.

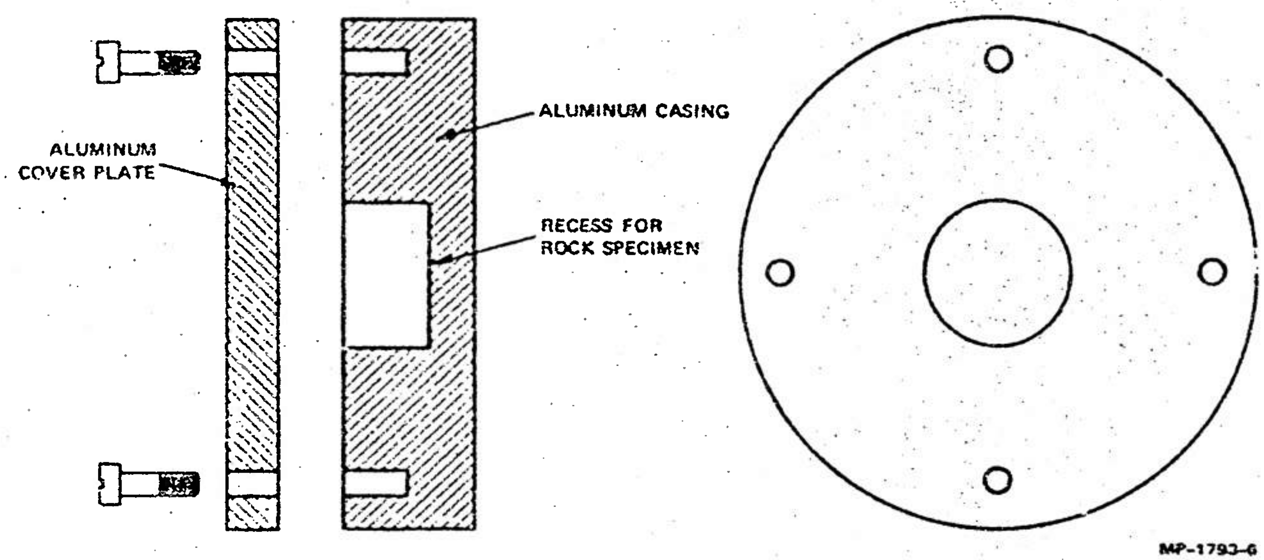

FIGURE 3 TARGET ASSEMBLY USED TO STUDY FRAGMENTATION OF ROCK UNDER DYNAMIC TENSILE LOADS

Table 2

FRAGMENTATION EXPERIMENTS

Experiment No.	Specimen Orientation	Impact Velocity (m/sec)	Computed Peak Tensile Stress (MN/m^2)	Remarks
44	P	30.0	83.8	Aluminum encasement carefully removed; specimen badly cracked and fell apart in large fragments.
45	P	20.8	58.1	Aluminum encasement carefully removed; specimen cracked but intact: subsequently sectioned, incipient crack coalescence.
46	P	19.0	53.1	Sectioned; incipient crack coalescence.
47	P	16.4	45.8	Sectioned; incipient crack coalescence.
48	P	14.8	41.4	Sectioned; no cracking.
49	P	16.4	45.8	Sectioned; isolated cracks.
50	P	17.1	47.7	Sectioned; isolated cracks.
51	N	17.4	48.6	Sectioned; isolated cracks.
52	P	49.5	138.0	Sectioned and mounted in epoxy to keep fragments from falling out; severe cracking, coalescence, and fragmentation.
53	N	48.9	136.0	Aluminum encasement carefully removed; specimen fell apart; sieve analysis performed.

Notes: P = specimen orientation was such that preexisting flaws lay roughly parallel to the impact direction.
N = specimen orientation was such that preexisting flaws lay roughly normal to the impact direction.
All specimens were cylinders 6.35 mm thick by 12.7 mm in diameter fully encased in aluminum as described in the text. Specimens 52 and 53 were impacted on the aluminum cover; all others were impacted on the casing side.

The next three experiments, 47, 48, and 49 were performed at stress levels near the dynamic tensile strength to determine whether the aluminum encasement arrangement caused significant stress amplitude attenuation. If so, impact velocities sufficient to cause incipient spall fracture in unencased specimens would not result in damage when encased. Experiments 47 and 49 performed at an impact velocity of 16.4 m/sec produced significant cracking, whereas experiment 48 at 14.8 m/sec produced no damage. These results are in agreement with the damage threshold velocity of 15.1 ± 0.8 m/sec established for unencased novaculite in the first annual report,[1] and so we conclude that the aluminum encasement had little attenuating effect on the stress.

Specimens 50 and 51 were to be impacted at about 25 m/sec, in the velocity range of advanced stages of crack coalescence and incipient fragmentation, but unfortunately much lower velocities, about 17 m/sec, were attained and much less damage resulted than was desired. The final two specimens were shock-loaded at significantly higher velocities to produce detached fragments. The aluminum casing (Figure 3) was impacted by the flyer plate in the first eight experiments. In Experiments 52 and 53, however, the specimen assembly was oriented such that the cover plate side was impacted.

The recovered targets were prepared for fractographic observation and analysis in one of two ways. Either they were cut carefully on a diameter to reveal the cracking pattern on a cross section, or else the aluminum encasement was removed by carefully machining the periphery down to a few mils in a lathe and subsequently dissolving the remaining few mils of aluminum in a 50% HCL solution.

In Situ Observations

Specimens 45 through 52 were sectioned and polished to reveal the cracking patterns. The effect of stress level on the extent of cracking is illustrated in Figure 4, which shows cross sections of specimens impacted at various velocities. The characteristic dome-shaped crack pattern is evident. Damage is usually heaviest in the half nearer the impact surface. Fine particles seem to be produced at midthickness and in the zone encompassed by the dome cracks. Large fragments originate mainly near the flat surfaces. The free-surface side of the specimen is usually least damaged and is often recovered in one piece, even when the remainder of the specimen has fragmented. Free, uncoalesced crack tips are commonly observed in specimens impacted at high as well as at low stresses.

Fragment Size Distribution

We attempted to determine the fragment size distributions produced in Experiments 44, 45, and 53 by carefully removing the aluminum encasements. Specimen 44, however, fell apart in only a few large pieces and was unsuitable for a sieve analysis. Specimen 45 remained intact after removal of the aluminum and retained considerable strength (firm hand pressure was insufficient to break it up), so it was mounted in epoxy and sectioned as described in the previous discussion.

The fragment size distribution for Specimen 53 was determined by placing the collected fragments in the top sieve of a series of U.S. sieves placed in the following order from top to bottom: No. 6, 8, 10, 14, 20, 40, 50, 100, 200, and 400, and a pan to catch the fines. The system was vibrated for a short time, and the particles retained on each screen were counted and weighed. Figure 5 shows the shapes of the particles; the raw data are presented in Table 3 and in Figure 6. These experimental fragmentation data were used to develop and check the dynamic fracture model.

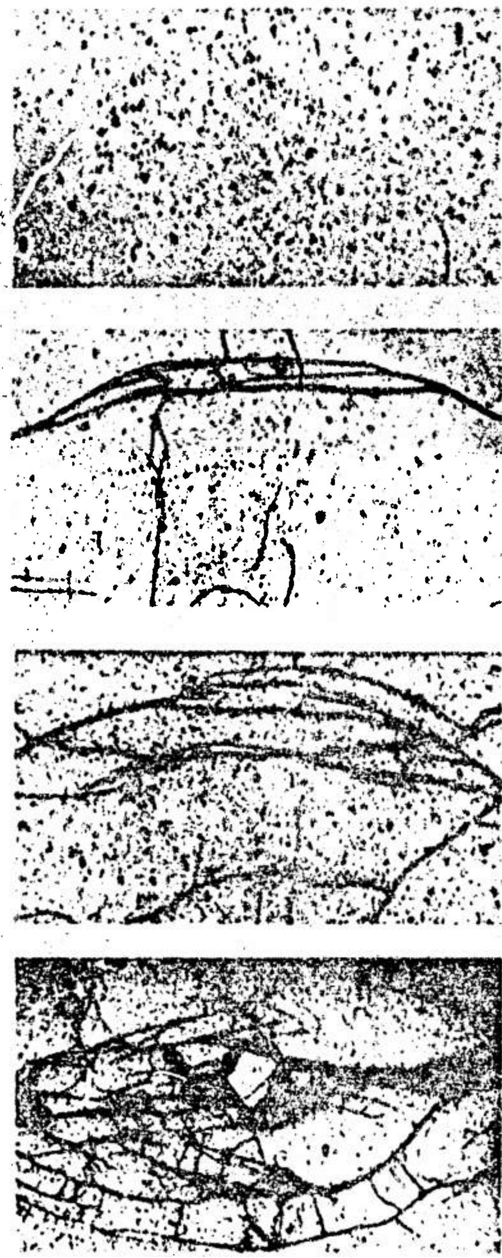

(a) EXPERIMENT 48
41.4 x 10^6 PASCAL

(b) EXPERIMENT 47
45.8 x 10^6 PASCAL

(c) EXPERIMENT 46
53.1 x 10^6 PASCAL

(d) EXPERIMENT 52
138 x 10^6 PASCAL

MP-1793-7

FIGURE 4 POLISHED CROSS SECTIONS OF ARKANSAS NOVACULITE SPECIMENS SHOWING THE EXTENT OF FRACTURE DAMAGE PRODUCED AT INCREASING LEVELS OF DYNAMIC TENSILE STRESS

Impact direction was from top to bottom.

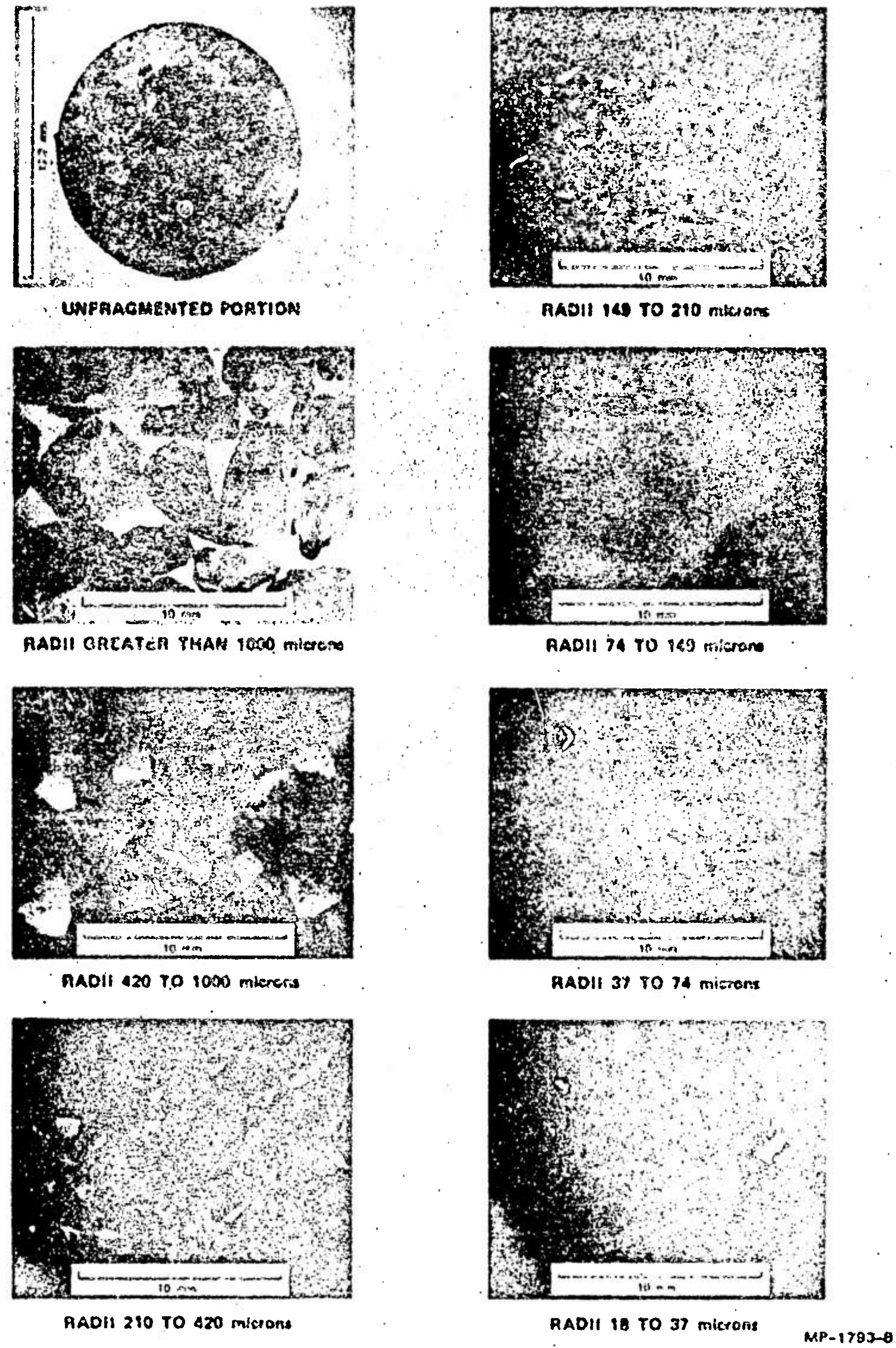

FIGURE 5 PHOTOMICROGRAPHS OF VARIOUS SIZED FRAGMENTS FROM EXPERIMENT 53

Table 3

SIEVE ANALYSIS RESULTS FOR ARKANSAS NOVACULITE: EXPERIMENT 53

U.S. Sieve No.	Sieve Opening (cm)	Sieve Half Opening (cm)	Weight of Retained Fragments (g)	Cumulative Weight of Retained Fragments (g)	Number of Retained Fragments	Cumulative Number of Retained Fragments	Cumulative Number of Retained Fragments per cm^3 (cm^{-3})
6	0.3360	0.1680	0.4894	0.4894	4	4	5.1
8	0.2380	0.1190	0.1778	0.6672	6	10	12.9
10	0.2000	0.1000	0.0755	0.7428	4	14	18.0
14	0.1400	0.0700	0.2095	1.0046	22	36	46.4
20	0.0840	0.0420	0.0811	1.0857	50	86	111.0
40	0.0420	0.0210	0.0645	1.1502	77	163	210
50	0.0297	0.0149	0.0163	1.1665	195	358	462
100	0.0149	0.0074	0.0123	1.1788	547	905	1168
200	0.0074	0.0037	0.0046	1.1834	727	1632	2105
400	0.0037	0.0018	0.0010	1.1844*	1204	2836	3660

Note: Specimen volume = 0.773 cm^3; specimen weight = 2.03 g.
* One large unfragmented piece weighed 0.8457 g.

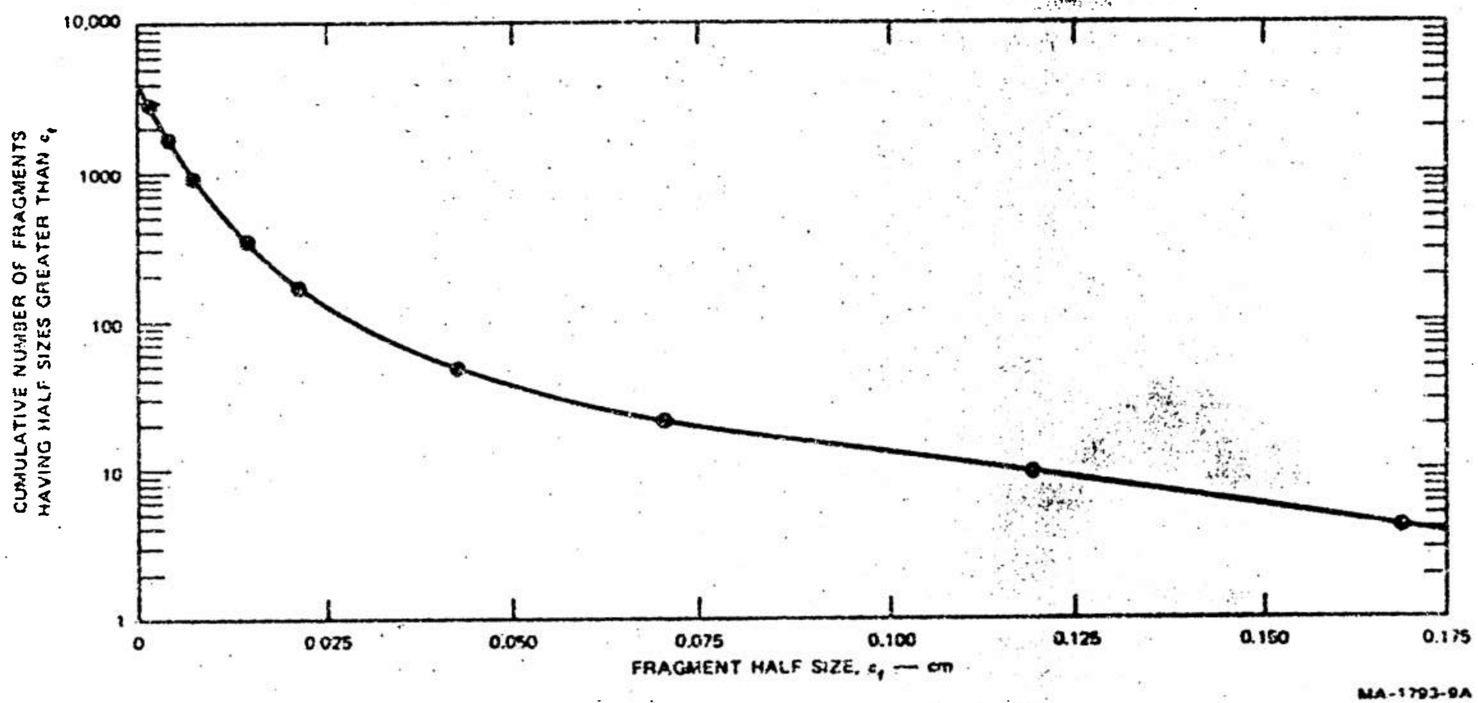

FIGURE 6 MEASURED FRAGMENT SIZE DISTRIBUTION FOR EXPERIMENT 53

Stress Wave Measurements

In fourteen experiments, an attempt was made to measure stress wave profiles transmitted through the specimen.[1] In addition to providing the peak stress and stress duration experienced by the rock under impact loads, measured stress histories yield important information about the constitutive relations and rate dependence. In the case of a specimen undergoing fracture, recompression waves emitted as microcracks form, impinge on, and reload the gage to an extent proportional to the dynamic tensile strength of the rock. Furthermore, the slope of the reloading pulse gives an indication of the rate of fracture--a sharp rise corresponds to brittle behavior.

Ytterbium piezoresistant stress gages mounted in plexiglass blocks were held in contact with the rear surface of the specimen. Upon impact, compressive waves impinge on the gage and the stress-induced electrical signals are recorded with an oscilloscope. The tensile stresses in the rock specimen are then calculable from the gage record, if the relative shock impedance of specimen and backing material are known.

The actual oscilloscope record obtained in these experiments, as well as a more detailed account of this stress wave-measuring technique, can be found in reference 1. The results may be summarized by noting that clear and consistent differences in the gage records were observed for specimens which underwent fracture. Therefore it was possible to tell whether or not a specimen was cracked before actually examining it. Peak compressive stresses experienced by the specimens, however, were not measurable from the gage records because of significant deviations from planar impact and hence excessive rounding of the oscilloscope traces.

III THE MECHANISM OF FRAGMENTATION

Considerable importance is attached to establishing the fragmentation mechanism, because this forms the basis for the computational model. The fragmentation mechanism is defined as that sequence of events that occurs in the rock during loading and leads up to fragmentation. We constructed the computational model for predicting fragment size distributions by modeling individually the physical processes that precede fragmentation. A model developed on such a physical basis should be inherently more accurate as well as more applicable to other materials under other loading conditions than a model based on, say, empirical correlations. Thus, each impacted rock specimen was examined carefully in search of evidence concerning the physical processes involved in fragmentation.

Fractographic Techniques

Two main fractographic techniques were used to deduce the fragmentation mechanism from impacted specimens. In one technique fracture surfaces and individual fragments were examined by optical and scanning electron microscopy to look for markings that would reveal how the surfaces and fragments were formed. These observations provided information on the histories of individual cracks. The other technique entailed stopping the fragmentution process at various stages of completion through careful control of the experiment, then sectioning the specimen, and examining the pattern of cracks intersecting the section. This technique yielded insight into the behavior of interacting cracks.

Fractographic Observations

The purpose of optical and scanning electron microscope examinations of fracture surfaces was to look for inhomogeneities that could have served as crack initiation sites, and river lines and hesitation lines which indicate the nature of crack growth.

As is typical of most rocks, the fractured surfaces were nearly featureless and for the most part yielded little evidence of how fracture occurred. The broken surfaces consisted of countless, well-defined and equisized polygonal blocks--quartz grains exposed by the passage of a crack along the grain boundaries. Only infrequently were propagation markings and hesitation lines observed. The circular markings in Figures 7a and b are known as hesitation lines because they are produced when the crack undergoes a sudden change of velocity as, for instance, when the crack is impinged upon by a stress wave. They are analogous to the arrest lines formed where a crack has actually stopped. Thus hesitation lines and arrest lines delineate the position of the crack front at some instant in time and thereby reveal the contour of the propagating crack. From the appearance of the hesitation lines in Figure 7, we deduce that the cracks had circular peripheries, i.e., they were penny-shaped.

Also evident on the fracture surface in Figure 7a are several lines radiating outward from the apparent center of the circular hesitation line and intersecting the hesitation line at right angles. These lines are actually height discontinuities and thus are reminiscent of river lines and cleavage steps commonly observed on fracture surfaces of metallic and ionically bonded materials. As such they form parallel to the propagation direction and thus indicate the propagation direction. Thus the river lines provide a running history of the crack path and a hesitation line gives the crack shape at an instant in time. Figure 7 is therefore interpreted to mean that crack propagation in novaculite under dynamic uniaxial strain loading occurs by the expansion of penny-shaped cracks radially outward from initiation sites.

A corollary of the fact that river lines form parallel to the crack propagation direction is that the fracture origin may be located by following the lines in a direction opposite to the propagation direction.

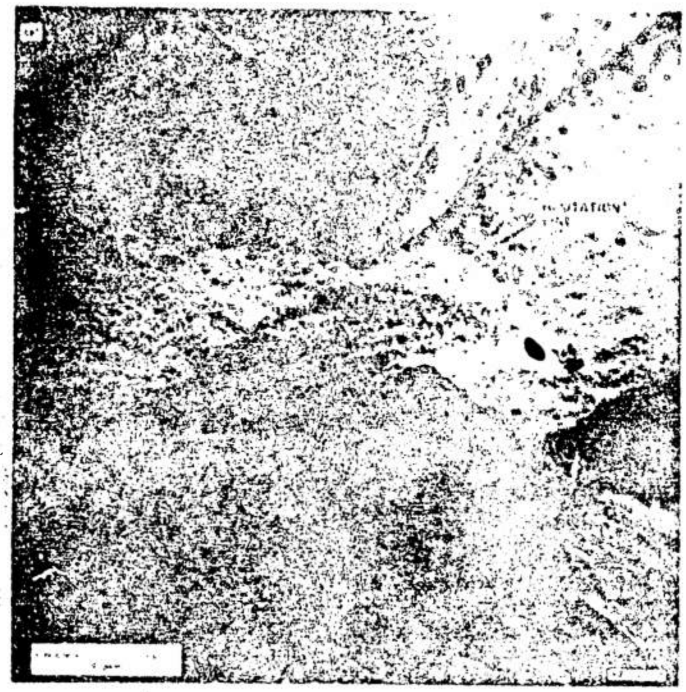

FIGURE 7 SECTIONS OF CIRCULAR HESITATION LINES ON THE FRACTURE SURFACES OF DYNAMICALLY LOADED NOVACULITE

Figure 7 shows clearly that the river lines emanate from a single site situated at the approximate center of the circular hesitation line. High resolution examination of this site with the scanning electron microscope did not reveal any obvious heterogeneity that might have served as the weak spot. In fact in no instance was it possible to identify positively the heterogeneity in the rock responsible for the initiation of a crack at that particular place. Thus we can only speculate that the heterogeneities responsible for crack initiation were the small crack-like flaws that existed inherently in the rock. The nature of these flaws is described more fully in Chapter V.

Individual fragments such as those shown in Figure 5 were also examined with optical microscopes. Their shapes as can be seen from the figure are roughly equiaxed, as opposed to elongated bodies as might perhaps be expected from Figures 4b and 4c. In general the fragments had from 6 to 8 facets, regardless of fragment size, implying that on the average 3 to 4 cracks are associated with one fragment, and indicating that larger cracks produce larger fragments whereas smaller cracks produce smaller fragments. It was also noted that individual fragments generally contained a number of cracks in their volumes, which means that not all cracks were effective in producing fragments.

The purpose of performing impact experiments at stresses insufficient to produce fragments, was to provide specimens for observation that contained various degrees of prefragmentation fracture damage. Such specimens were cut carefully on a diameter with a diamond saw, and this surface was polished to reveal a cross section of the cracking pattern and to provide in situ views of fragmentation. Figure 4 shows the appearance of four such specimens impacted at stress levels ranging from one below the tensile strength through one sufficient to produce loose fragments. This figure may also be viewed as depicting successive stages in time of a fragmenting rock specimen, i.e., as the stress in the wave rises, increasingly more cracks originate and grow.

These pictures show that cracks initially form near to the impact surface and propagate predominately in the lateral direction (normal to the direction of the maximum tensile stress). At low stresses, few fragments can form, and they are large. As the stress level increases, more cracks are initiated and more coalescence occurs. Crack growth does not appear to be particularly sensitive to stress level. Only at the highest stress (Figure 4d) can significant numbers of vertical cracks be seen. The effect of the vertical cracks is clearly to increase the extent of specimen comminution. They transform the large elongated fragments (Figure 4c) to many smaller, more equiaxed fragments (Figure 4d) and thus influence strongly the resulting fragment size distribution.

Figure 4d also indicates that smaller fragments tend to originate near the mid-thickness of the specimens whereas the larger fragments came from the material near the impacted and free surfaces.

Hypothesized Fragmentation Mechanism

From these observations we envision a mechanism of fragmentation consisting of four stages, namely:

(1) Activation of a number of preexisting structural flaws

(2) Propagation of activated cracks radially outward

(3) Coalescence and branching of propagating cracks

(4) Isolation of individual rock fragments from one another.

The first two stages have been verified by similar impact experiments on a transparent material. Figure 8 shows the internal penny-shaped cracks produced in this material, a polycarbonate. The tiny black areas that are observable at the center of every crack have been positively identified as inherent flaws in the material produced during fabrication. The multiple concentric rings visible on the crack surfaces in polycarbonate are similar to the hesitation lines found on novaculite fracture surfaces and imply that the crack morphology in novaculite should be basically penny-shaped and should remain penny-shaped during growth until coalescence begins.

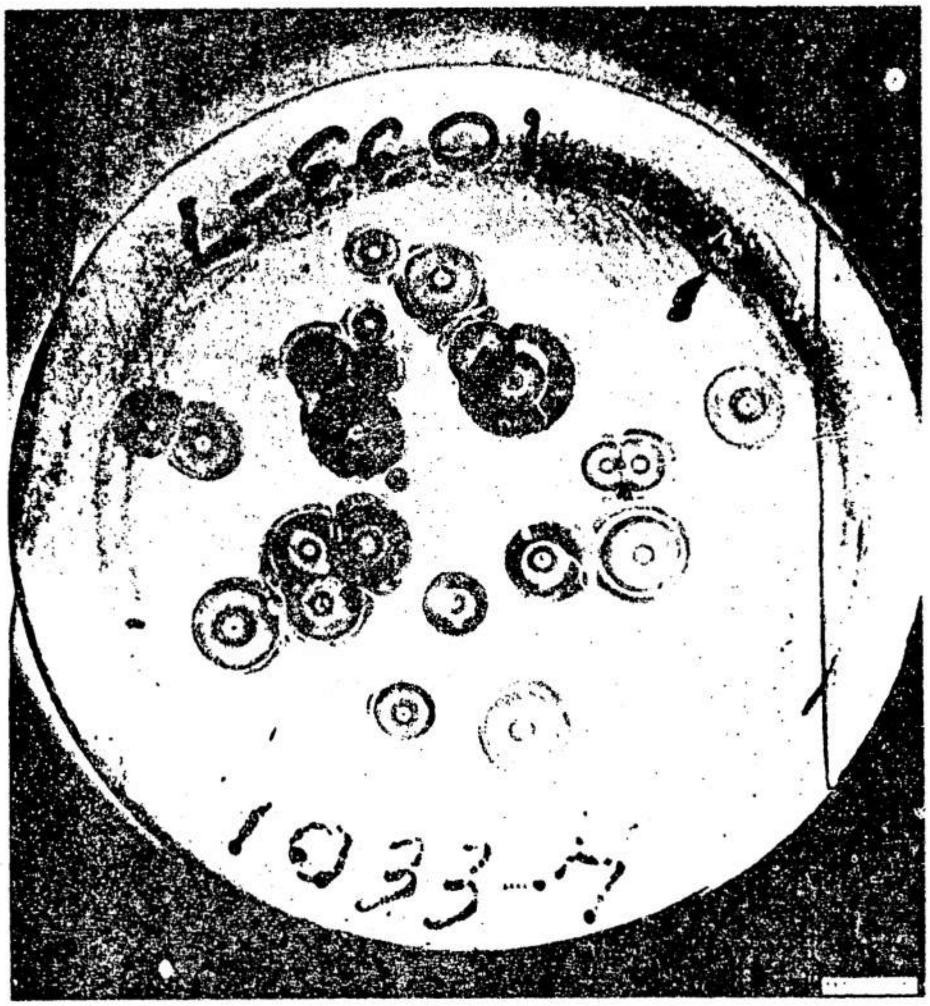

FIGURE 8 INTERNAL CRACKS IN A TRANSPARENT POLYCARBONATE PRODUCED BY SIMILAR DYNAMIC LOADS

IV CONSTRUCTION OF THE PREDICTIVE CAPABILITY

The capability for predicting the fragment size distribution for novaculite under dynamic one-dimensional-strain loads was obtained by combining a computational model of the fragmentation mechanism with a finite difference wave propagation code. The computational fragmentation model is based on the fragmentation mechanism hypothesized in the previous chapter, and treats quantitatively each of the four stages, namely; flaw activation, crack growth, crack coalescence, and fragment formation. The one-dimensional wave propagation code, PUFF,[4] calculates from the impact conditions the stress history in the specimen, i.e., the magnitude and duration of the stress at any point in time.

The Computational Fragmentation Model

The fragmentation of novaculite under dynamic, one-dimensional-strain conditions is modeled by treating quantitatively the hypothesized stages of the fragmentation mechanism. A treatment of each of the four stages is given below.

Activation of preexisting flaws--Based on experimental observations of impacted and unimpacted Arkansas novaculite (Chapters III and V, respectively) we assume that the material contains inherently a population of penny-shaped flaws of varying sizes, some of which become unstable upon passage of the stress wave and develop into propagating cracks. To calculate the number of flaws activated by a given stress pulse (and hence the number of cracks in the material) we invoke a Griffith-Irwin fracture mechanics criterion,[5,6] i.e., flaws having a radius c larger than some critical size that is a function of the tensile stress $c^* = c^*(\sigma)$ will be activated, whereas those flaws smaller than c^* remain dormant. Of the various crack geometries for which fracture mechanics stress analyses exist, Sneddon's[7] relation for an internal penny-shaped crack in an infinite elastic medium subjected to a uniform tensile stress normal to the crack plane

$$c^* = \pi K_{Ic}^{\;2}/4\sigma^2 \qquad (1)$$

most nearly applies to the conditions of our experiments, i.e., the cracks appear to be roughly penny-shaped, and the specimen behaves as if it were infinite during the life of the tensile pulse. The plane strain fracture toughness K_{Ic} for novaculite is determined in the following chapter. Thus we use Eq. (1) to calculate the size of the smallest flaw which will be activated by a dynamic load. To obtain the number of activated flaws, we need to know the size distribution of flaws in the rock. This has been measured for novaculite and the results are presented in Chapter V.

Crack Propagation--The distance which each crack can propagate depends on the crack velocity and the duration of the stress pulse. We assume here that the cracks accelerate very rapidly to a constant maximum velocity of one third the longitudinal wave speed. This is in accord with our experimental observations (Chapter V) as well as with theoretical estimates.[8-11] Knowing that crack propagation occurs radially outward from activation sites, the fracture surface area produced per crack at any given time step can be approximated by

$$A_i(t) \cong 2\pi(C_\ell \Delta t/3)^2 \qquad (2)$$

providing the crack was not stopped prematurely by barrier to crack growth or coalescence with other cracks. Individual cracks arrest when the stress level falls below the value given by Eq. (1). Thus the total fracture surface area produced in novaculite by a known stress pulse of peak stress σ and duration Δt insufficient to cause significant coalescence is given by

$$A_{total} \cong \frac{2N_{act}}{3} (C_\ell \Delta t)^2. \quad (3)$$

where N_{act} is the number of activated flaws.

Furthermore, the total energy absorbed in creating new surface area can be estimated if the specific fracture surface energy γ is known.

$$E_{fracture} \cong \frac{2\gamma N_{act}}{3} (C_\ell \Delta t)^2 \quad (4)$$

Crack Coalescence--Our quantitative treatment of coalescence of propagating cracks entailed assuming a criterion for the distance between converging cracks at which interaction first occurs, and taking a statistical approach by treating large numbers of coalescing cracks.

To develop the coalescence criterion, the concept of the "crack range" is introduced. The crack range $\tau_c(c)$ is defined as the volume of solid material surrounding a crack that experiences magnified strains of some arbitrary level, which arise from the stress concentrating effect of the crack. When the crack ranges of two cracks overlap, they are considered to have coalesced. As an upper limit (obtained from the solution of the elastic stress field around a penny-shaped crack in an infinite medium) the crack range includes the material within one crack radius of any part of the crack. Thus for a penny-shaped crack the maximum crack range is an ellipsoidal volume of revolution shaped like a hamburger. The volume then is

$$\tau_c(c) = (\pi^2 + \frac{10}{3}\pi)c^3 \cong 20.34\ c^3 \quad (5)$$

The observation that the fragments are nearly equiaxed suggests a much smaller crack range volume. For instance if the fragments were cube-shaped, then the crack ranges would be the volumes of two small pyramids on either side of each crack (one crack forming one side of the cube) and the crack range volume is

$$\tau_c(c) = \frac{8}{3} c^3 \qquad (6)$$

For our purposes we will define T_c by

$$\tau_c(c) = T_c c^3 \qquad (7)$$

where T_c will probably lie between 2 and 20.

We can now postulate a coalescence criterion. It is logical that two propagating cracks in an infinite body have no knowledge of one another until they come within some critical distance of each other. When this critical nearness is attained, the cracks sense each other and interaction begins. The concentrated stresses at each crack front superimpose, and the propagation behavior of each crack is influenced by the presence of the other. In the present experiments the crack tip stresses are similar and therefore should be additive, thereby encouraging the cracks to propagate into each other and coalesce. The extent of the strain field about a crack is given by its range as previously defined, and we presume that crack coalescence occurs when the ranges overlap. For numerical computations with the wave propagation code we adopt the following coalescence criterion: crack coalescence occurs when the sum of the crack range volumes for all the cracks in a finite difference cell is equal to the volume of that cell. This criterion may be expressed mathematically as follows:

Consider a distribution of penny-shaped cracks whose size distribution is given by $\rho_c(c)$, the density of cracks as a function of size.

The cumulative crack density N_g^c (the number of cracks per unit volume with radii greater than c) is given by

$$N_g^c = \int_c^\infty \rho_c(c)dc \qquad (8)$$

Recalling the definition of the crack range $\tau_c(c)$, we can write the expression for the relative volume of material influenced by the cracks per unit volume

$$V_\tau = \int_0^\infty \tau_c(c)\ \rho_c(c)\ dc. \qquad (9)$$

The coalescence criterion then may be simply stated as

$$V_\tau = 1 \qquad (10)$$

Fragment Formation--After a certain degree of crack coalescence, fragments of various sizes will form. The fragment sizes will reflect in some way the crack size distribution which led to the fragmentation. The procedure for determining whether fragments have formed is to compute the volumes of the fragments which would be formed by the cracks which exist. If the fragment volumes fill the volume of the finite difference cell, then complete fragmentation has occurred. Otherwise, the fracture calculations continue. Preparatory to introducing the procedure for computing the number of fragments, the fragment size distribution, the fragment volume, and the relations between the crack and fragment variables are defined.

Let the fragment size distribution be described by $\rho_f(c)$, a density of fragments associated with the crack radius c. As for cracks, the continuous size distribution is represented in the computer program by a discrete set of size groups

$$\Delta N_i^f = \int_{c_i}^{c_{i+1}} \rho_f(c)\,dc \qquad (11)$$

Here we note that the fragment size distribution is a function of the radii of the cracks, not of the fragments. Let $\tau_f(c_f)$ be the volume of the fragment with fragment radius c_f. This volume may be written

$$\tau_f(c_f) = T_f c_f^3 \qquad (12)$$

where T_f is, for example $4\pi/3$ for spherical particles and 8.0 for cubes.

The fragment volume will just fill the total volume at the time of complete fragmentation. Therefore the fragmentation criterion is

$$V_T^f = \int_0^\infty \rho_f(c)\ \tau_f(c_f)\ dc = 1 \qquad (13)$$

or

$$V_T^f = \sum_i \Delta N_i^f\ \tau_f(c_f) = 1 \qquad (14)$$

To determine the number and size of fragments, we introduce the following relations between crack and fragment variables.

$$\rho_f' = V_r \beta \rho_c(c) \qquad (15)$$

$$c_f = \gamma\ c \qquad (16)$$

where β and γ may be functions of c, and V_r is the remaining relative volume which has not been fragmented by cracks larger than c.

For 8-sided fragments where each face is formed by one crack, $\beta = 1/4$ and $\gamma = 1.0$.

The procedure for computing the fragment size distribution and for determining whether fragmentation has occurred begins with $V_r = 1.0$. First, the largest cracks are transformed to fragments using Eq. (15). These fragments have a volume

$$V_I^f = \Delta N_I^f T_f \gamma^3 c_I^3 \tag{17}$$

in the computer program. This volume V_I^f is presumed to contain small cracks which do not form fragments. Therefore, to compute the fragments for the next smaller crack size, this volume is removed before computing the number of fragments of the next smaller size. In general, the number of fragments is

$$\Delta N_i^f = \beta \Delta N_i^c V_r \tag{18}$$

where $V_r = 1 - \sum_{j=i+1}^{I} V_j^f$.

This process for determining the number of fragments is followed until all activated cracks are treated or until all the volume is full of fragments. If all the volume is filled with fragments, then the cell is presumed to be completely fragmented.

At the end of the computation the material that contains coalescing cracks but is not fully fragmented is taken as partially fragmented. The number of fragments of each size is determined by the foregoing calculation. The remaining unfragmented material is not assigned to any fragment size group, but is assumed to be part of one of the large chunks observed in the experiments.

Stress History Calculations

PUFF, a one-dimensional, finite difference wave propagation code[4] was used to calculate the magnitude and duration of the stress at every location in the specimen and at every point in time. It also calculates the current density and energy. Because of the low stresses required to produce fragmentation, the Hugoniot elastic limit is never exceeded and plastic behavior is never realized. Therefore a very simple equation of state, Hooke's law, can be used to calculate the stresses in novaculite. The equation of state for plexiglass is well known.[12] The PUFF code has been used successfully to predict wave profiles in a number of materials under known conditions of one-dimensional impact (Reference 13, for example).

The simple elastic equation of state for novaculite is no longer adequate for describing the material response once the fragmentation process begins. When cracks begin to form and grow, the apparent elastic stiffness decreases. Recompression waves run out from the surfaces of the propagating crac : to interact with and erode the stress pulse. This effect is of considerable magnitude, and must be taken into account in the calculations.

The procedure used to determine the stiffness of material undergoing fracture and fragmentation has been given elsewhere.[13] The basis of the method is the concept of a two-component system: solid material, and void inside the open cracks. The specific volume of the system changes when loaded: this change is due partially to the solid and partially to the change in the void volume. The void volume calculation follows the analysis of Sneddon[7] for a penny-shaped crack in an elastic material. During the wave propagation calculation, the following sequence of events may occur while the material is in tension:

(a) Initial tensile loads cause only elastic volume changes in the solid until a threshold stress (equal to the dynamic fracture strength) is reached.

(b) When the stress exceeds the fracture threshold, cracks begin to nucleate and grow, and the void volume produced by the cracks acts to decrease the volume change required of the solid. Thus the tensile stress in the solid is lower than it would be for undamaged material under the same volume change; hence, the effective modulus of the solid has decreased.

(c) With increasing stress and continuing volume change, a point is reached where the void volume increase just equals the applied volume change. Here there is no change in solid volume and hence no change in tensile stress: the stress-volume path has reached a peak and the effective modulus is zero.

(d) With further volume changes the increase of void volume (by growth and nucleation of cracks) tends to exceed the applied volume change. Then the solid volume change is negative and the tensile stress is decreasing. The effective modulus is negative during this period.

(e) If compressive volume changes occur at any time, there will usually be a decrease in both void volume and solid volume. Then the effective modulus is positive as in (a).

(f) If no net volume change occurs, there will usually be an increase in void volume and a corresponding decrease in solid volume: the effective modulus in such a case is infinite.

The preceding sequence of events is treated in the present formulation of the behavior of material undergoing fracture. A derivation of the effect of damage on the material stiffness is given below to indicate the basis of the method. Here the case is considered in which no growth or nucleation of cracks occurs: the resulting modulus is that which is appropriate for a residual strength calculation. The fundamental relation is that the total volume change is the sum of solid and void volume changes:

$$\Delta V = \Delta V_s + \Delta V_v \qquad (19)$$

The void volume change is derived from the analysis of Sneddon[7] for the opening of a penny-shaped crack in an elastic medium under uniform tension. The half-opening of the crack faces is

$$\delta = \frac{4(1-\nu^2)c\sigma}{\pi E}$$

where c is the half crack length

σ is the stress applied normal to the crack plane

E is Young's modulus

ν is Poisson's ratio.

The void within the crack faces is an ellipsoid with semiaxes c, c, and δ, so the volume is

$$V_c = \frac{4}{3}\pi\,\delta c^2 = \frac{16(1-\nu^2)\,c^3\sigma}{3E} \qquad (20)$$

To determine the total crack volume a sum is made over all cracks.

$$V_v = \sum_i N_i V_{ic}$$

where N_i is the number of cracks of volume V_{ic} per unit volume. Then Eq. (19) becomes

$$\frac{\Delta V}{V} = \frac{\Delta\sigma \cdot V_s}{(K + \frac{4}{3}\mu)V} + \frac{16(1-\nu^2)\Delta\sigma}{3E}\,N_i c_i^3 \qquad (21)$$

where $\Delta\sigma$ is a change in stress

K, μ are bulk and shear moduli

V is the total specific volume.

Dividing Eq. (21) by $\Delta\sigma$, an effective modulus M is derived.

$$\frac{1}{M} = \frac{V_s/V}{K + \frac{4}{3}\mu} + \frac{16(1-\nu^2)}{3E} N_i c_i^3 \qquad (22)$$

This compliance is similar to that which would be obtained for a composite made of solid material plus void. The term $K + \frac{4}{3}\mu$ is the stiffness of the solid and V_s/V is its volume fraction. The last term on the right in Eq. (22) must be interpreted then as the compliance of the cracks. This expression shows that the compliance of the composite increases with increasing void fraction, i.e., increasing number and/or increasing size of cracks.

V ROCK PROPERTIES

Execution of the predictive capability described in the previous chapter requires a knowledge of certain rock-specific properties, for their values are required as input. Included are the size distribution of inherent flaws, the plane strain fracture toughness, and the crack growth velocity. Values of these parameters for Arkansas novaculite are determined in this chapter.

Inherent Flaw Structure

Casual observation with the unaided eye of polished novaculite surfaces is sufficient to show that this rock has a strongly oriented flaw structure. The flaw structure is clearly evident in the low magnification composite micrograph of Figure 9. The size distribution of the inherent flaws was determined by counting and measuring the flaw traces on a polished section through a specimen. Those data, which represented the size distribution of flaw traces per unit area, were then converted by means of a statistical transformation to obtain the actual size distribution of inherent flaws per unit volume.

Nine overlapping photographs at 40X were required to span the diameter of a rock specimen. The total photographed area was slightly more than 1.1 cm^2, and in this area 194 preexisting crack traces were counted and measured. These data were converted by means of a Scheil type statistical transformation[14,15] implemented by the BABS2 computer code;[16] the results are presented in Figure 10.

Here the cumulative concentration of cracks having radii greater than radius c_i is plotted as a function of c_i. The relatively few (194) traces observed on about 1 cm^2 of the surface of section transform into a very large volume density (~100,000/cm^3). The size distribution of preexisting cracks has a parabolic form in log-normal space with a cut-off at about $c = 500$ µm. The curve is well described by the analytical

Preceding page blank

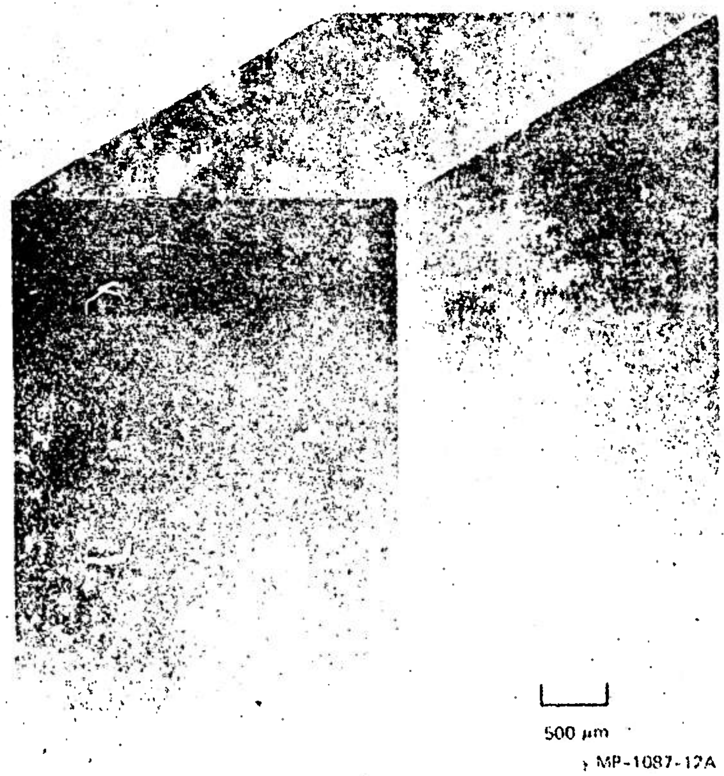

FIGURE 9 COMPOSITE MICROGRAPH OF A BLOCK OF NOVACULITE SHOWING THE PREFERRED ORIENTATION OF THE INHERENT FLAWS

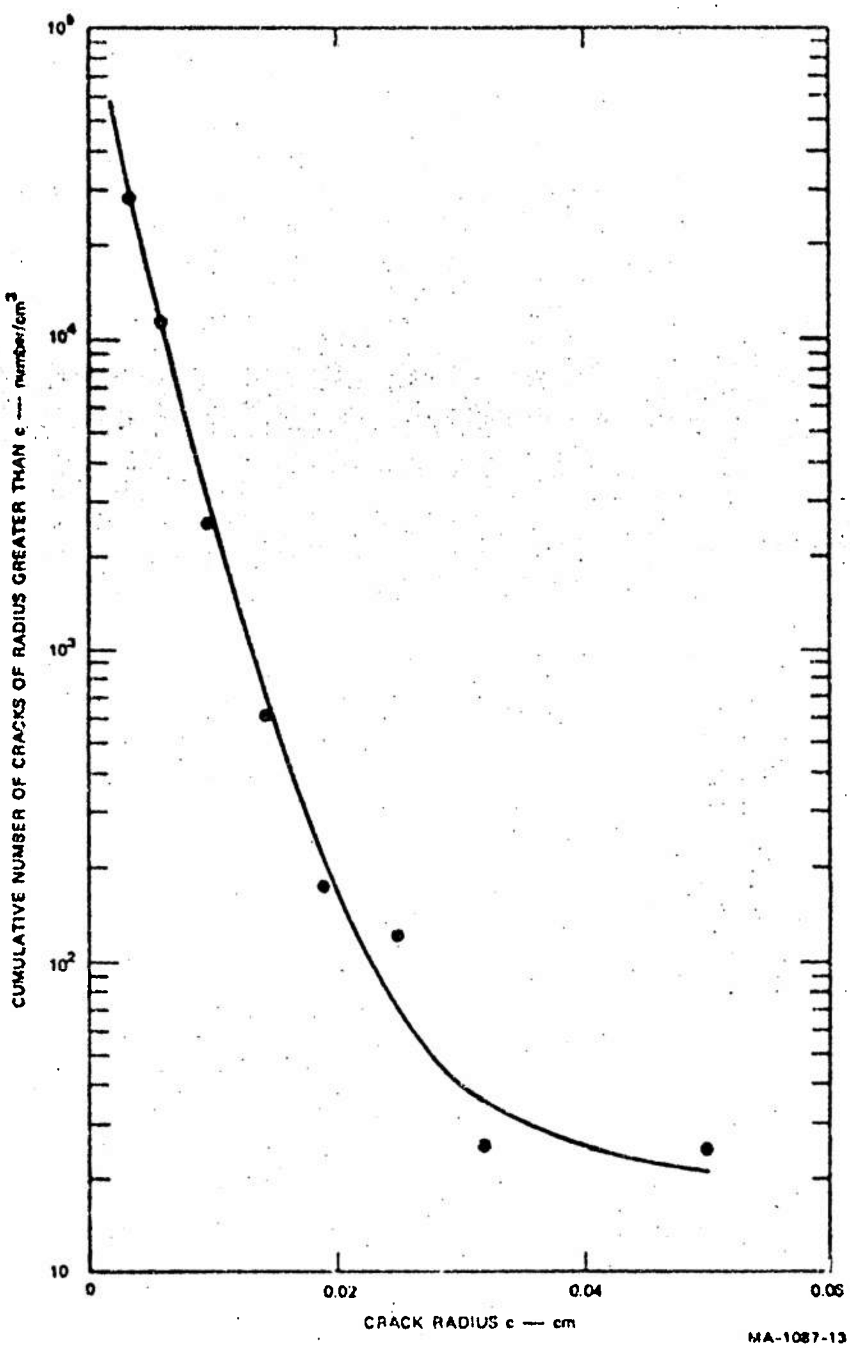

FIGURE 10 CUMULATIVE SIZE DISTRIBUTION OF INHERENT FLAWS IN ARKANSAS NOVACULITE

expression

$$N = \delta(c)\ \exp[11.1 - (3.7 \times 10^2)c + (0.42 \times 10^4)c^2] \quad (23)$$

where $\delta(c) = 1$ for $0 < c \leq 0.05$

$\delta(c) = 0$ for $c > 0.05$

and c is in centimeters.

The cutoff in crack half size at about 500 um appears to be realistic. A very large number of observations of polished novaculite surfaces were made, and never were flaw traces significantly greater than 1 mm observed. Statistically speaking if many observations of crack traces are made, the length of the largest trace is approximately equal to the diameter of the largest flaw. Thus the radius of the largest inherent flaw in the present specimens of Arkansas novaculite was taken to be about 500 μm.

Fracture Toughness

The plane strain fracture toughness K_{Ic} is a material property that describes the resistance of the material to crack propagation. This parameter is used in the first stage of the fragmentation model to determine the critical flaw size for a given dynamic stress and hence the number of inherent flaws in novaculite that became propagating cracks.

The dynamic plane strain fracture toughness for novaculite was calculated from the measured dynamic tensile strength of 41.0±2.0 MN/m^2 (5950 ±290 psi) (Chapter II) and the radius of the largest flaw, 500 μm, established in the previous section. Sneddon's expression, Eq. (1), is used to relate the dynamic tensile strength σ_f and the radius of the largest penny-shaped flaw c_{max} to the dynamic fracture toughness K_{Ics}.

$$K_{Ics} = 2\sigma_{\ell}\sqrt{\frac{c_{max}}{\pi}}$$

and a value for K_{Ics} of 1.04 $MN/m^{3/2}$ is obtained. Quasi-static tensile strength determinations using the SRI expanded ring tests[1] yielded similar values for the tensile strength and hence the fracture toughness, demonstrating that these properties of novaculite are strain rate-insensitive, at least for strain rates in the range of 3×10^{-4} sec^{-1} to 7×10^{3} sec^{-1}.

Crack Velocity

The distance each crack can propagate depends on the crack velocity and the duration of the stress pulse. Ytterbium stress gages were used to measure the latter in this work and crack velocities were inferred from direct measurements of the distance propagated by cracks in essentially crack-free material. The radii of the cracks shown in Figure 2 are about 2 mm. The ytterbium stress gage records indicated that the stress duration was about one microsecond, in agreement with the result obtained from simple calculations using the measured elastic wave speed and the thicknesses of the specimen and flyer plate. Thus crack propagation velocities of 2×10^{5} cm/sec are indicated--an interesting result, since it is approximately one-third of the measured longitudinal wave velocity for novaculite, and is thus in agreement with theoretical estimates of the maximum crack velocities of brittle materials.[8-11] Materials such as Armco iron and beryllium, investigated in other projects,[13,16] fractured in a brittle manner at high strain rates, but exhibited viscous crack propagation and maximum crack speeds well below $c_{\ell}/3$.

VI COMPARISON OF PREDICTED AND EXPERIMENTAL RESULTS

A test of the predictive capability of the model was made by calculating the fragment size distribution of Experiment 53, and then comparing the predicted result with the experimentally measured result.

Experimental Conditions

Experiments 52 and 53 were carried out under identical conditions (Table 2). Both novaculite specimens were encased in aluminum to retain the fragments, and both were impacted at a velocity of about 49 m/sec. Specimen 52 was sectioned afterwards to reveal the location of cracks and fragments (Figure 4d), whereas the aluminum encasement was carefully removed from Specimen 53 and the size distribution of the fragments was determined (Figures 5 and 6).

In both experiments the novaculite specimens were bonded on the impact side to the aluminum with epoxy; the rear surface however was unbonded, and it appears therefore that a gap perhaps 10 to 30 μm wide existed there. It was not realized at the time of the experiment how critical the gap at the rear interface would be, and consequently no steps were taken to either eliminate or measure the gap. Subsequent wave propagation calculations, however, showed that the presence of a gap has a large influence on the location and magnitude of the peak tensile stresses and, therefore, on the fracture behavior.

Calculational Conditions

Computations made at stress levels below that required for fracture for the situation where a bond existed at the rear interface predicted a peak tension of about 160 MN/m^2 (23,200 psi), which first appeared near the rear interface. For the situation of an unbonded interface with no gap, a peak tension of 100 MN/m^2 (14,500 psi) occurred first near the interface and dropped off rapidly as a gap formed. For the

Preceding page blank

case where an initial gap existed at the interface, the rear face of the specimen behaved as a free surface, and tensile stresses of about 100 MN/m^2 (14,500 psi) were predicted throughout the specimen thickness, arising first at about one-third of the specimen thickness from the rear interface. This last stress distribution is in accord with the cracking patterns observed in Figure 4d, and so we assumed in calculating the fragment size distribution for Experiment 53, that a 0.0025-cm gap existed at the rear interface.

In attempting to predict the fragment size distribution for Experiment 53, we assumed 8-sided fragments and fragment sizes equal to the sizes of the cracks at the time of coalescence, i.e., we let $\beta = 1/4$ and $\gamma = 1.0$. The calculation was stopped after five reverberations of the tensile waves.

Predicted versus Observed Results

The results of the calculations are presented in Figure 11, which shows that fragmentation occurred at three positions through the specimen thickness. The coalescence criterion was chosen by comparing this computed result with the observed crack patterns of Figure 4. This comparison indicates that the total crack range volume for coalescence should be about 3 cm^3, which implies a value for T_c of $\pi/3$. In view of our previous estimates of the T_c parameter in Chapter IV, this value is somewhat low, but several calculations with different values of T_c show that there is no significant effect on the fragment sizes. Rarefaction waves interacted to produce tension first near Cell 40, and the stress duration was sufficiently long that enough crack growth occurred for the total crack range to equal the cell volume. Hence Cell 40 fragmented. During the third tensile reverberation, Cell 44 fragmented and during the fifth, Cell 21 also fragmented. Cell 22, which exceeded the coalescence condition by nearly as much as Cell 21, did not reach the fragmentation condition. Thus the calculations predict two heavily fractured positions in the vicinity of each face of the specimen--a prediction that is in reasonable accord with the experimental result as shown in Figure 4d.

Although the fracture pattern in Specimen 52 (Figure 4d) was predicted well by the code calculation, the agreement may be somewhat fortuitous. Whereas the calculations showed cracking and fragmentation occurring first at two locations near the rear surface and later at locations nearer the impact surface, the series of micrographs of Figure 4 implies that cracking occurs first near the impact surface and later near the rear surface. Thus if the micrographs of Figure 4 may be thought of as a time sequence, the experimental observations are opposite from the fracture behavior predicted by the code.

To compute the fragment size distribution, the fragments in all the cells were summed. In Cells 21, 40, and 44, the fragments were counted and sized as described in Chapter IV. In the other cells, where the total crack range did not meet the fragmentation criterion but did meet the coalescence criterion, we computed the fragments in the usual way and disregarded the unfragmented material. The computed fragment size distribution is presented in Figure 12, where the distribution measured experimentally is also given for comparison.*

The calculated and experimental curves in Figure 12 do not coincide, but they are qualitatively alike. Agreement concerning the sizes of the large fragments is good, and the curves have the same shape for intermediate-sized fragments. There appear to be too many computed fragments

---

* We attempted to obtain an extra point on the experimental curve by measuring the radii of the three largest fragments. This point is included in Figure 12 and used to guide the extension of the experimental curve (broken line). The three largest fragments weighed 0.4367 g.

in the range of $c \approx 0.03$ cm. This suggests that changes should be made in either the growth or fragmentation process for the smaller size cracks. The cutoff in the computed distribution curve at small fragment sizes exists because no fragments were computed for those sizes since inherent flaws smaller than about 0.02 cm were not activated.

No attempt was made to repeat the calculations using different values of β and γ. However, it is likely that better agreement could be obtained, and it would be valuable in future work to study the consequences of variations in these parameters for cases where more experimental data are available.

The above fracture and fragmentation model applies only to uniaxial strain loading conditions. However, the generalization to two dimensional axially symmetric loading geometries such as those obtaining in many blasting and drilling situations is possible, and is in fact currently in progress under Contract DAAD05-73-C-0025 with the Ballistic Research Laboratory, Aberdeen, Maryland.

In this report all incipient flaws are assumed to lie normal to the direction of wave propagation. However, our present fracture model allows an initial flaw orientation distribution which is maintained during propagation. In this case the driving and opening stress for a given crack is the component normal to the crack. This option was not exercised in the present work because the incipient flaws nearly all lay in a plane normal to the direction of wave propagation.

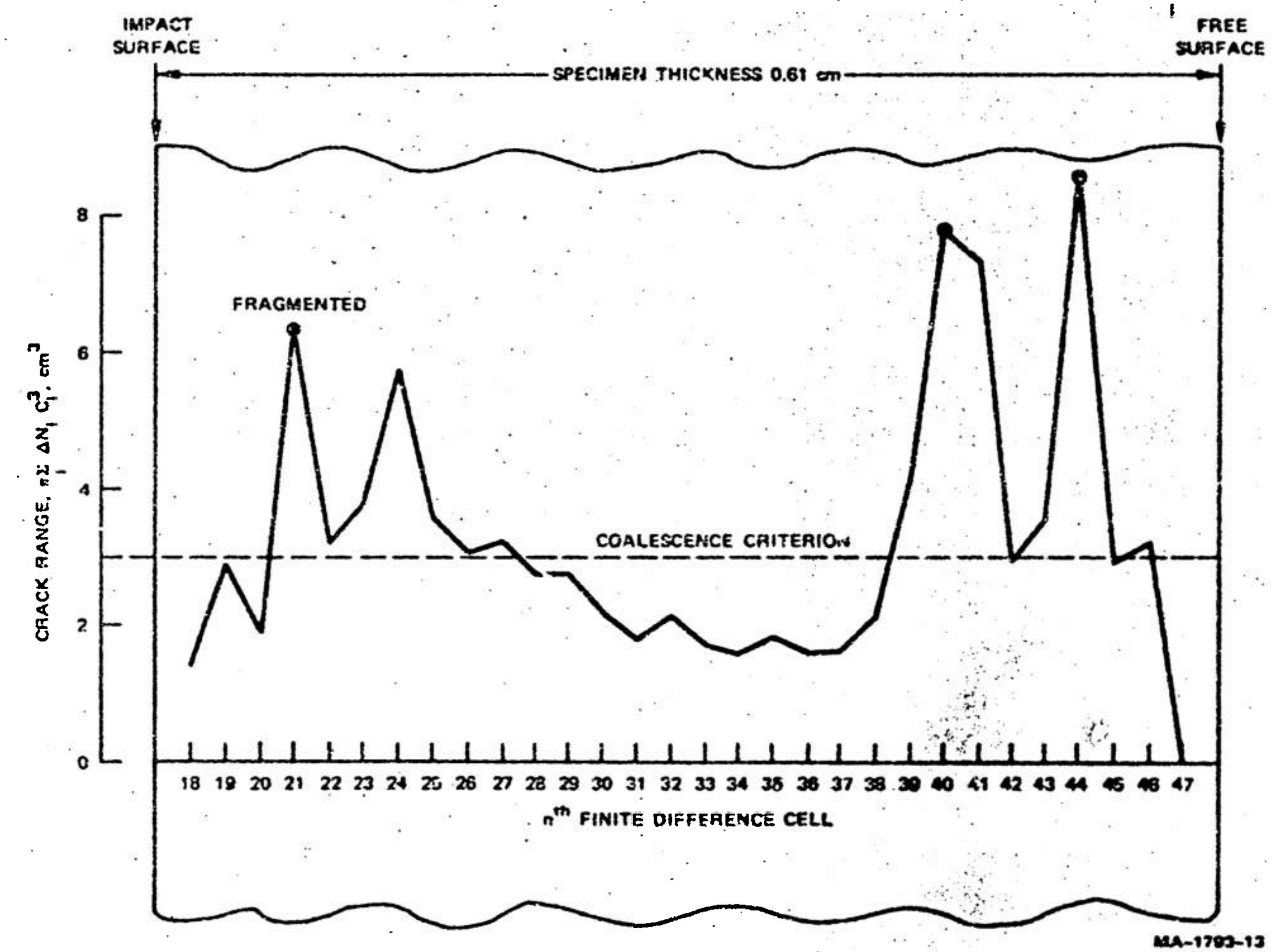

FIGURE 11 VARIATION OF COMPUTED TOTAL CRACK RANGE WITH POSITION FOR SPECIMEN 53

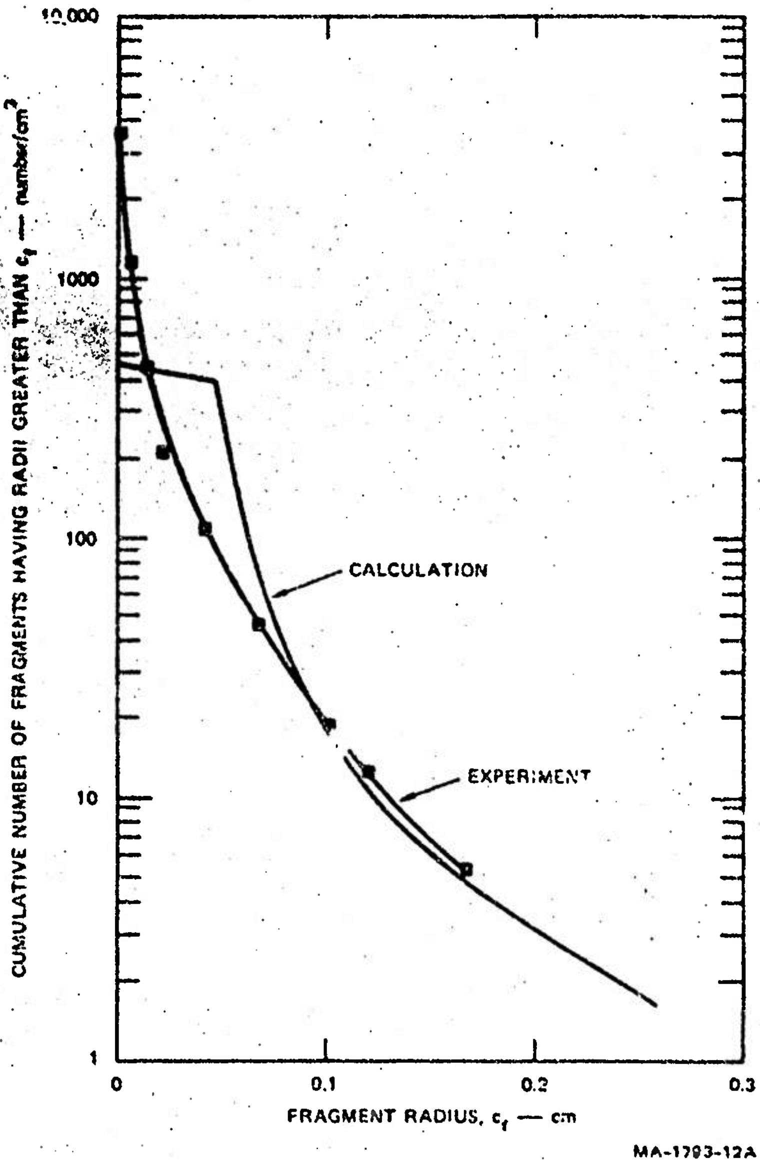

FIGURE 12 COMPARISON OF EXPERIMENTAL AND COMPUTED FRAGMENT SIZE DISTRIBUTIONS FOR EXPERIMENT 53 IN ARKANSAS NOVACULITE

REFERENCES

1. Shockey, D. A., C. F. Petersen, D. R. Curran and J. T. Rosenberg, "Dynamic Tensile Failure in Rocks," Annual Technical Report to the U.S. Bureau of Mines, Contract No. H0210018, March (1972).
2. Shockey, D. A., C. F. Petersen, D. R. Curran, and J. T. Rosenberg, "Failure of Rocks Under High Rate Tensile Loads," New Horizons in Rock Mechanics, p. 709, Proc. 14th Symp. on Rock Mech. eds., H. R. Hardy, Jr., and R. Stefanko, Amer. Soc. Civil Engrs. New York, NY (1973).
3. Curran, D. R., D. A. Shockey, and L. Seaman, "Dynamic Fracture Criteria for Polycarbonate," J. Appl. Phys. (to be published Sept. 1973).
4. Seaman, L., "SRI PUFF 3 Computer Code for Stress Wave Propagation," Technical Report No. AFWL-TR-70-51, Air Force Weapons Laboratory, Kirtland AFB, New Mexico, September (1970).
5. Griffith, A. A., "The Phenomena of Rupture and Flow in Solids," Phil. Trans. Roy. Soc. London A221, 163 (1920).
6. Irwin, G. R., "Onset of Fast Crack Propagation in High Strength Steel and Aluminum Alloys," Proceedings 1955 Sagamore Conference on Ordnance Materials, Vol. II (Syracuse University Press, New York, 1956).
7. Sneddon, I. N., "The Distribution of Stress in the Neighborhood of a Crack in an Elastic Solid," Proc. Roy. Soc. London A187, (1946).
8. Mott, N. F., "Fracture of Metals: Some Theoretical Considerations," Engineering, 165, p. 16 (1948).
9. Roberts, D. K., and A. A. Wells, "The Velocity of Brittle Fracture," Engineering 178, 820 (1954).
10. Dulaney, E. N. and W. F. Brace, "Velocity Behavior of a Growing Crack," J. Appl. Phys. 31, 2233 (1960).

11. Berry, J. P., "Some Kinetic Consideration of the Griffith Criterion for Fracture - Parts I and II," J. Mech. Phys. Solids 8, 194-216 (1960).

12. Barker, L. M., and R. E. Hollenbach, "Shock Wave Studies of PMMA, Fused Silica, and Sapphire," J. Appl. Phys. 41, 4208-4226 (1970).

13. Shockey, D. A., L. Seaman, and D. R. Curran, "Dynamic Fracture of Beryllium Under Plate Impact and Correlation with Electron Beam and Underground Test Results," Contract F29601-70-C-0070, AFWL-TR-73-12, Air Force Weapons Laboratory, Kirtland AFB, New Mexico, January 1973.

14. Scheil, E., "Die Berechnung der Anzahl and Grossenverteilung kugelformiger Kristalle in undurchsichtigen Korpern mit Hilfe durch einen ebenen Schnitt erhaltenen Schnittkreise," Z. Anorg. Allgem. Chem. 201 (1931).

15. Scheil, E., "Statistische Gefügeuntersuchungen I," Z. Metallk. 27, 199 (1935).

16. Barbee, T., L. Seaman, and D. R. Curran, "Dynamic Fracture Criteria of Homogeneous Materials," AFWL-TR-71-156, Air Force Weapons Laboratory, Kirtland AFB, Albuquerque, New Mexico, December 1971.

17. Brace, W. F., E. Silver, K. Hadley, and C. Goetze, "Cracks and Pores: A Closer Look," Science 179, 162 (1972).

18. Sedlacek, R., "Tensile Fatigue Strength of Brittle Materials," Air Force Materials Laboratory, Wright Patterson AFB, Ohio, Technical Report AFML-TR-66-245, March 1968.

19. Sedlacek, R., and F. A. Halden, "Method of Tensile Testing of Brittle Materials," Rev. Sci. Instr. 33, 298 (1962).

20. Sedlacek, R., "Processing of Ceramics--Surface Finishing Studies," Final Technical Report, Stanford Research Institute, prepared for Naval Air Systems Command, Contract No. N00019-69-C-0229, April 1970.

21. Wawersik, W. R., and W. S. Brown, "Creep Fracture of Rock," Semiannual Technical Report, DARPA Contract No. H0220007 prepared for the Bureau of Mines, Twin Cities Mining Research Center, Twin Cities, Minnesota, July 1972.

22. Ginsberg, M. J., "Piezoresistance of Ytterbium and Calibration of Ytterbium Stress Transducers," prepared for Defense Advanced Research Projects Agency under DNA Contract No. DNA001-72-C-0146, Draft Final Report, June (1973).

APPENDIX I CHARACTERIZATION OF OTHER ROCKS

Four rock types* were used in this study. Arkansas novaculite was the material most completely investigated, but characterization work was also performed on Sioux (Jasper) quartzite, Holston limestone (Pink Tennessee marble), and Westerly granite. This section describes the microstructures and defect structures of the four rock types and presents the results of measurements of their physical and mechanical properties.

Microstructures

Figure 13 shows a polished surface of Arkansas novaculite that was etched for 2 minutes in 40% HF at room temperature to reveal the grain structure. Black areas are holes where inherent flaws intersect the surface or where grains have been removed during the polishing process; bright areas are caused by reflected light from internal flaw surfaces.

By exploiting the translucency of novaculite and focusing into the material to a depth of about 100 μm, we found that the inherent flaws exist predominately in two shapes: penny-shaped and pencil-shaped. Best results were obtained by viewing the specimens in reflected polarized light through a microscope slide and with an oil film of matching refractive index (n = 1.55) on the specimen surface. Figure 14 shows a penny-shaped and a pencil-shaped flaw slightly below the surface of polish and inclined at an angle to it, so that only a section of each is in focus. The planes of the rather homogeneously distributed penny-shaped flaws are roughly parallel to one another, and most of the pencil-shaped flaws are inclined at about 45 degrees to these planes.

One-inch cubes of Sioux quartzite, Westerly granite, and pink Tennessee marble were cut from the large blocks received from the

---

* Supplied by the Property Determination Research Support Group, Twin Cities Mining, Research Center, Bureau of Mines, Twin Cities, Minnesota 55111.

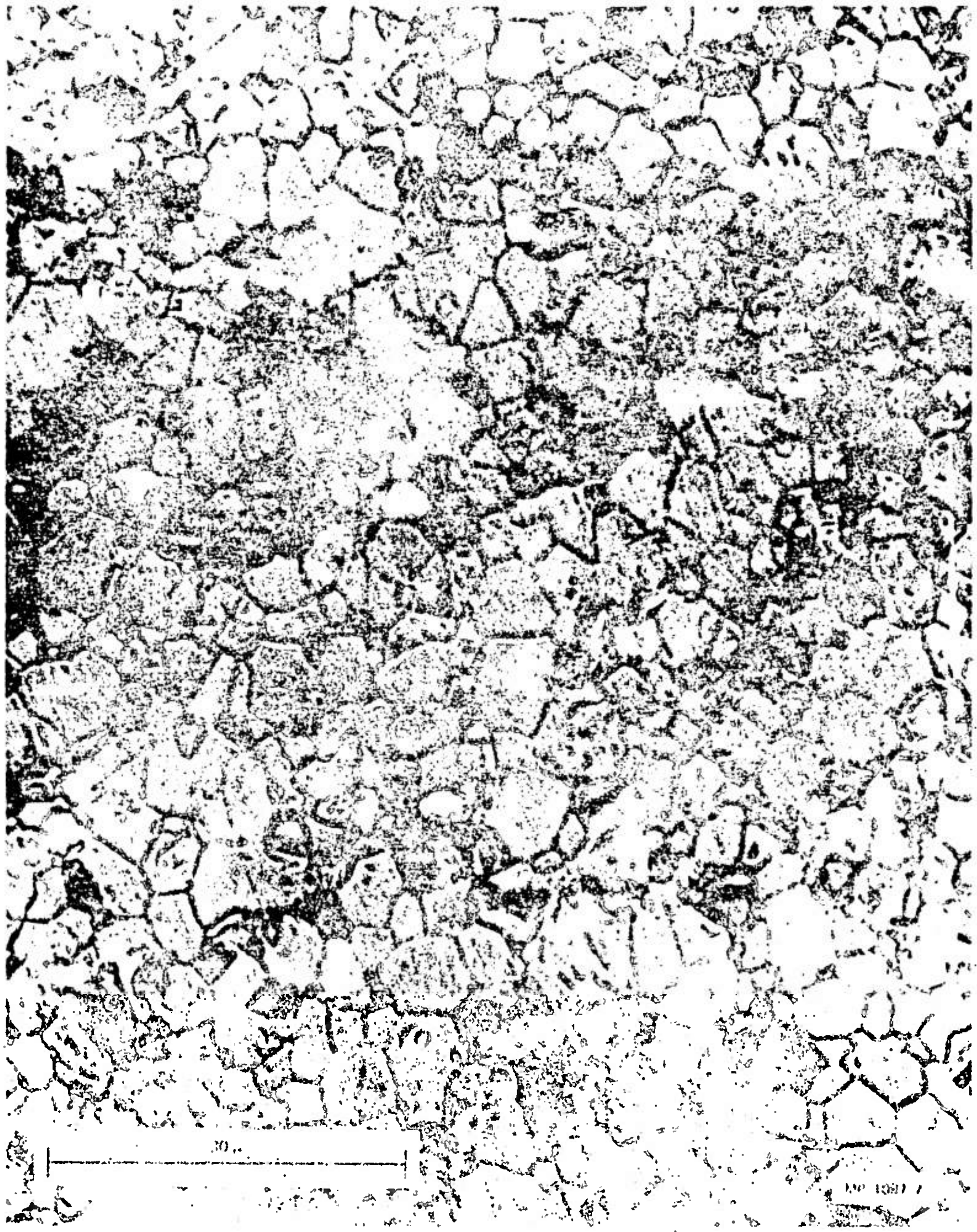

FIGURE 13 MICROSTRUCTURE OF ARKANSAS NOVACULITE SHOWING THE EQUIAXED QUARTZ GRAINS

Etched two minutes in an aqueous 30 percent HF solution.

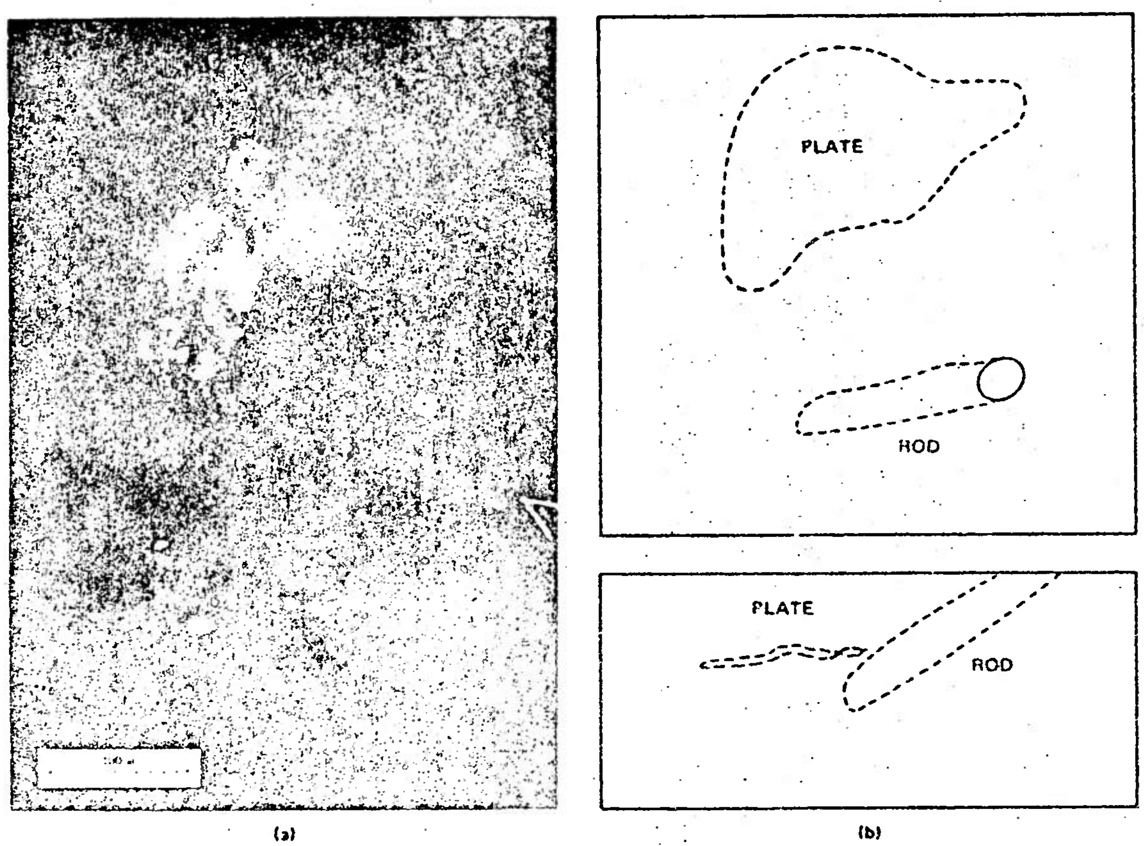

(a) PHOTOGRAPH WITH POLARIZED LIGHT

(b) SCHEMATIC DEPICTION

MP-1087-9

FIGURE 14 PENNY-SHAPED AND PENCIL-SHAPED INHERENT FLAWS IN NOVACULITE

Bureau of Mines and polished on three perpendicular sides in preparation for petrographic examination. Photomicrographs showing the grain structures of the three rock types are presented in Figure 15.

The Sioux quartzite is relatively pure, dense, and homogeneous. Large cracks, pores, and faults are noticeably absent. The grains are equiaxed, randomly oriented, and about 30 times larger than those in Arkansas novaculite (average grain diameter is of the order of 300μ).

As indicated by the pronounced relief of polished surfaces, Westerly granite consists of hard grains (quartz) in a softer matrix (microcline and plagioclase). The quartz grains are generally irregular with diameters often exceeding 1000μ. The dark biotite phase is randomly oriented.

The grain size in the marble ranged from very small (~10μ) to very large (3000μ) and was easily discernible in 3/4 polarized light. A large majority of the grains exhibited pronounced twinning. No preferred grain orientation was evident.

Inherent Flaw Structures

The inherent flaw structure of Arkansas novaculite was easily discernible, and it was possible by counting and measuring flaw traces on polished surfaces to determine quantitatively the inherent flaw size distribution. This effort was described fully in Chapter V. The inherent flaw structure of Sioux quartzite, Westerly granite, and pink Tennessee marble, however, was much more difficult to see. Nearly all flaws in these rocks are associated with grain boundaries and could be detected only by focusing painstakingly up and down with the optical microscope at magnifications greater than 100X. Occasional transgranular cracks were observed in the feldspar grains of the Westerly granite.

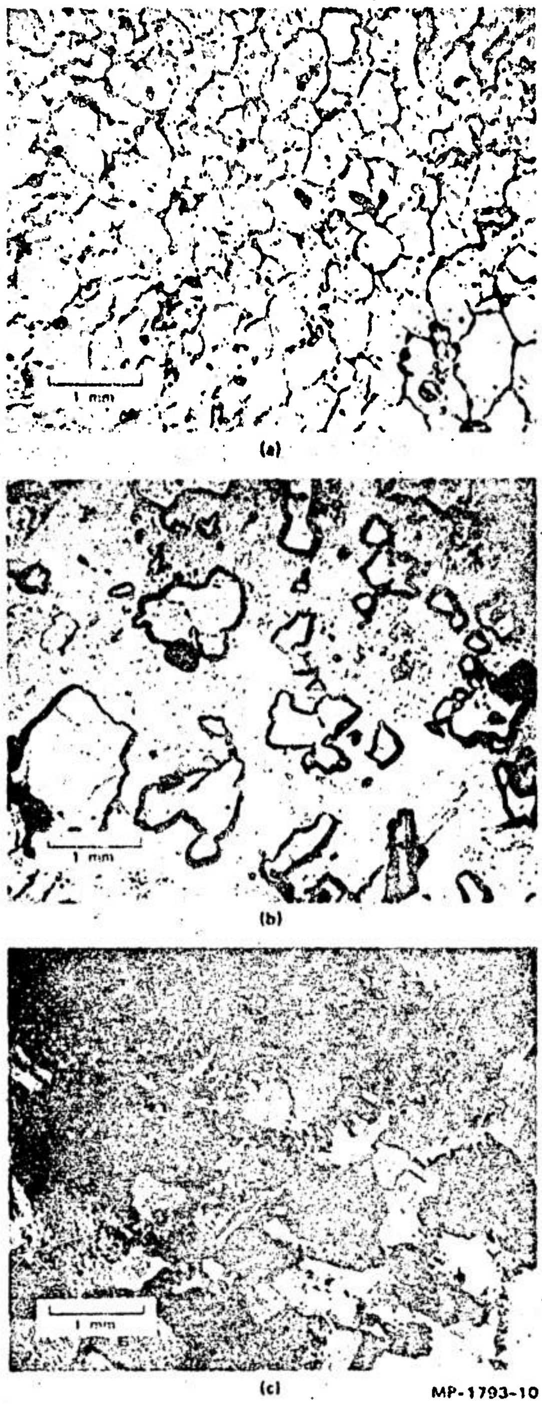

FIGURE 15 MICROSTRUCTURES OF (a) SIOUX QUARTZITE, (b) WESTERLY GRANITE, AND (c) PINK TENNESSEE MARBLE

Special viewing and crack decoration techniques were tried in attempting to observe the flaw structure. Phase contrast photography and scanning electron microscopy proved ineffective; likewise swabbing polished rock surfaces with silver nitrate and vacuum impregnation with an organic fluorescing agent to decorate the microcracks was of little use. Thermal grooving was not attempted, but seems of doubtful value since the flaws are associated almost exclusively with grain boundaries which themselves should be attacked by the thermal grooving process. It might be fruitful to attempt to relate grain size or some other readily observable characterizing parameter of the grain boundaries to the number, sizes, and shapes of crack-like defects between the grains.

A procedure recently reported by Brace at al.,[17] which uses ion thinning to reveal cracks in Westerly granite and Rutland quartzite, appears promising. However, we were not able to try it in this work.

Physical and Mechanical Properties

The density of each rock type was measured by an immersion technique and the longitudinal and transverse sound wave velocities were determined by the time-in-flight method. The results are given in Table 4. The density measurements were all near the theoretical value and indicated that porosities were less than 1%. The Young's moduli for the four rock types were calculated from the measured densities and sound speeds according to the relationship

$$E = \rho C_{\ell}^{2} \left[\frac{(1+\nu)(1-2\nu)}{(1-\nu)}\right] \quad (24)$$

where a value of 0.25 was assumed for Poisson's ratio, and the resulting values are included in the table.

Table 4

MEASURED PROPERTIES OF SEVERAL ROCKS

	Density (g/cm^3)	Longitudinal Sound Speed* (m/sec)	Transverse Sound Speed* (m/sec)	Elastic Modulus† (MN/m^2)	Quasi-static Tensile Strength (MN/m^2)
Arkansas Novaculite	2.63	5900	4030	9.15×10^4 (13.3×10^6 psi)	44.1±3.0 (6400±440 psi)
Sioux Quartzite	2.64	5030	3750	6.65×10^4 (9.64×10^6 psi)	18.3±2.3 (2660±230 psi)
Westerly Granite	2.65	4330	2860	4.92×10^4 (7.14×10^6 psi)	10.8‡ (1575 psi)
Pink Tennessee Marble	2.71	5670	3370	8.48×10^4 (12.3×10^6 psi)	8.18‡ (1185 psi)

* As measured by time-in-flight method.

† Calculated from Eq. 24 assuming a value of 0.25 for Poisson's ratio.

‡ Average values measured by Wawersik and Brown (Ref. 21) in a uniaxial stress test.

Quasi-Static Strength Measurements

The tensile strength of novaculite and Sioux quartzite under quasi-static loading conditions was determined using the SRI expanded ring test[18,19] shown in Figure 16. In this test hydrostatic pressure acts radially against the inside wall of a cylindrical specimen to create a uniform tangential tensile stress in the specimen wall. Non-axial stresses caused by misalignment and localized stress concentrations, which normally arise from gripping or supporting the test specimens, are eliminated in this method.

Ring-shaped specimens were diamond ground from oversized blanks to the following dimensions:

	Arkansas Novaculite	Sioux Quartzite
I.D. (mm)	50.8	81.4
O.D. (mm)	58.4	87.8 to 91.2
Height (mm)	7.62	26.4

All strength measurements were made at a strain rate of 3×10^{-4} sec^{-1}.

Measurements on novaculite were taken both in air and under a vacuum of 10^{-5} torr. Some materials show higher strengths under vacuum, indicating that stress corrosion is an important factor. No significant difference was seen for novaculite. Results of 15 tests in air indicated a tensile strength of 44.1 ± 3.2 MN/m^2 (6400 ± 440 psi) and 12 tests under vacuum indicated 44.9 ± 3.0 MN/m^2 (6500 ± 480 psi). The extremes measured were 50.7 and 38.6 MN/m^2. The results of nine tests on Sioux quartzite in air indicated a tensile strength of 18.3 ± 2.3 MN/m^2 (2660 ± 330 psi). Average values of the quasi-static tensile strength of Westerly granite and pink Tennessee marble have been reported by Wawersik and Brown to be 10.8 MN/m^2 (1575 psi) and 8.14 MN/m^2 (1185 psi), respectively.

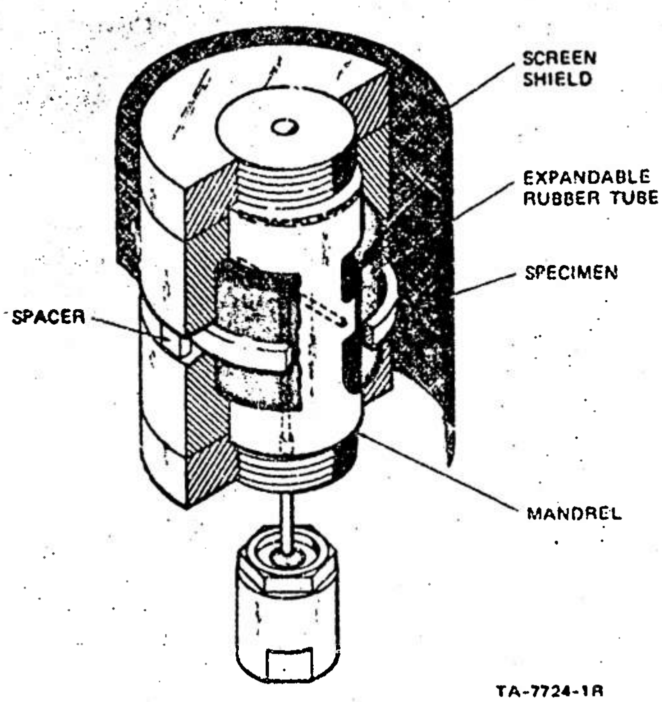

FIGURE 16 THE SRI EXPANDED RING TEST

It is noteworthy that the quasi-static tensile strength of novaculite is the same as the high strain rate tensile strength measured in the impact experiments in Chapter II. The strain rate of the dynamic tests was estimated from the oscilloscope records of the ytterbium stress gages in the instrumented experiments.[1] The rise time of the stress pulse is about a tenth of a microsecond, the elastic strain is about 7×10^{-4}, hence the strain rate is estimated to have been approximately 7×10^{3} sec^{-1}. Since this is more than seven orders of magnitude higher than the strain rates of the quasi-static ring tests, the negligible difference in strength values indicates that the fracture strength is strain-rate insensitive, at least in this range.

Stress Wave Measurements

Four attempts were made to measure the load history in specimens of Westerly granite that were impacted in the gas gun. The experimental conditions were similar to those described in Chapter II and Reference 1.

Small grid-like gages made of ytterbium were cemented to the back surfaces of the rock specimens and backed by a plexiglass plate. Because of the piezoresistive nature of ytterbium, a change in resistance is produced in the material when traversed by a compressive wave. This resistance change is measured and recorded by an oscilloscope as a change in voltage, and is subsequently converted to a record of stress versus time by means of an established calibration.[22] The tensile stress history in the rock specimen is then calculated from the measured compressive stress history in the plexiglass and the relative shock impedances of the two materials. (See the Appendix to the First Annual Report).

Four specimens of Westerly granite, 10 cm square by 0.625 cm thick, were impacted by flat plexiglass flyer plates 0.165 cm thick at velocities of 27.4, 123, 36.9 and 41.0 m/sec. The impact velocities were chosen such that stresses in excess of the dynamic tensile strength were obtained. The purpose was to record the "fracture signal," a second hump on the stress gage record caused by impingement on the gage of recompression waves emanating from internal surfaces as cracks form and grow. In all four experiments, the impact was too nonplanar to yield analyzable results.

Figure 17 gives the measured stress history at the rear surface of specimen 1260 impacted at 41 m/sec. A clear fracture signal was recorded, but nonplanarity of impact resulted in a triangular rather than a flat-topped initial compressive wave, and therefore a direct and unambiguous determination of the dynamic tensile strength of Westerly granite is not obtainable from this record. However, the peak compressive stress was calculated for this experiment, and using the results of this record an upper limit on the dynamic tensile strength of Westerly granite was determined to be 47 MN/m^2 (6800 psi).

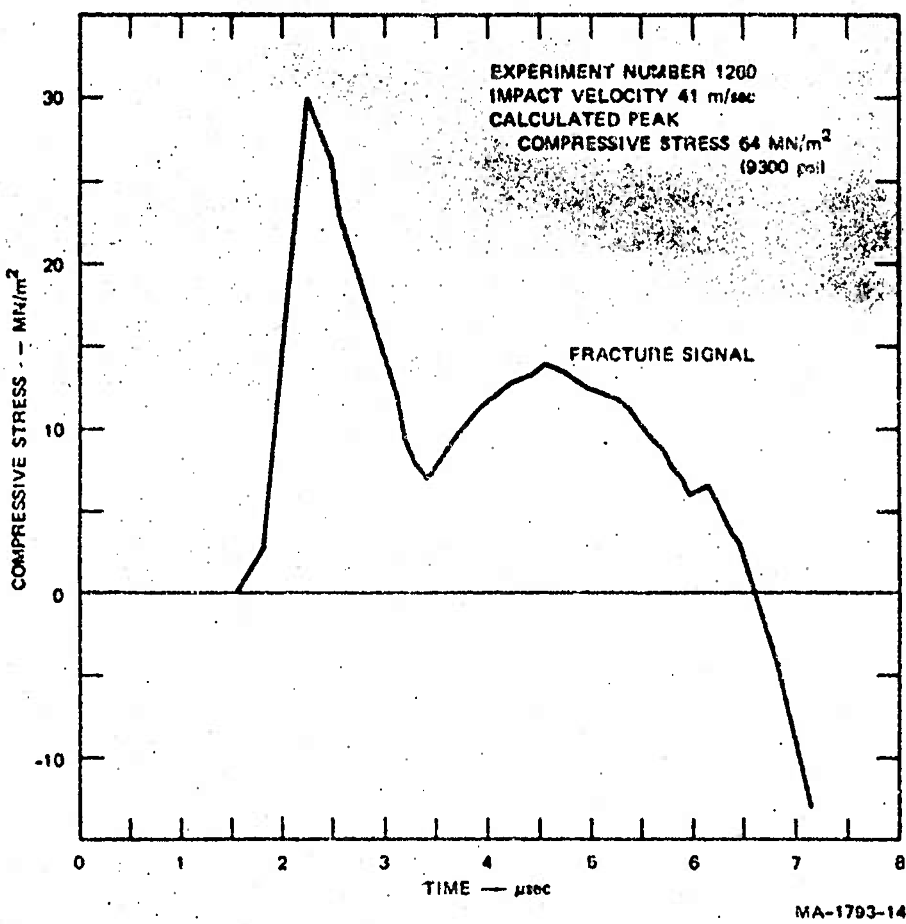

FIGURE 17 EXPERIMENTAL STRESS HISTORY NEAR THE REAR SURFACE OF A WESTERLY GRANITE SPECIMEN MEASURED WITH AN YTTERBIUM STRESS GAGE

Form DI-1216
(June 1968)

UNITED STATES
DEPARTMENT OF THE INTERIOR

Date June 1973

SUMMARY REPORT OF INVENTIONS AND SUBCONTRACTS

The following report must be submitted in *triplicate* as part of the interim or final report as provided for by the REPORTS and/or PATENT ARTICLE in the grant or contract.

Name of Contractor or Grantee	Address
STANFORD RESEARCH INSTITUTE	333 Ravenswood Avenue, Menlo Park, California 94025

Contract or Grant No.	H0220053

(Check appropriate boxes)

1. Type of Report:

☐ Interim { From ...., 19...... / To ...., 19...... }

☒ Final.

2. Interim Report Data:

A. Invention made ☐, not made ☐, during interval of (1).

B. If invention(s) made, provide the following information:

☐ Previously fully disclosed in Invention Disclosures. Give dates submitted, and Contractor's docket numbers.

☐ Invention Disclosures attached herewith. Give Contractor's docket numbers.

(OVER)

3. Final Report Data:

	Date Submitted	Contractor's Docket Number
A. Invention(s) previously reported—		
B. Invention(s) reported herewith—		

C. Others (explain)—

4. Patent application(s) filed and contemplated to be filed by Contractor under the terms of the grant or contract:

Application Serial No. . .					
Date of filing					
Contractor's Docket No. . .					

5. If this is a final report and no inventions were made under the grant or contract, certify as follows:

I certify that there were no inventions conceived or first actually reduced to practice in the work called or required under the grant or contract identified herein.

Date June 28, 1973

Signature

Title Physicist

6. Subcontracts containing patent rights article:

☒ None. ☐ Listed below are subcontractors not previously identified.

Name of Subcontractor	Address	Subcontract Number	Date Executed
(1)			
(2)			
(3)			
(4)			

7. Attach a copy of the patent rights article employed in each subcontract set forth in 6.

U.S. GOVERNMENT PRINTING OFFICE : 1955—O 222-087